Monthly Notices
of the
ROYAL ASTRONOMICAL SOCIETY

MNRAS **437,** 458–474 (2014)
Advance Access publication 2013 November 2

doi:10.1093/mnras/stt1901

Reversal or no reversal: the evolution of the star formation rate–density relation up to $z \sim 1.6$

F. Ziparo,[1,2]⋆ P. Popesso,[1] A. Finoguenov,[1,3,4] A. Biviano,[5] S. Wuyts,[1] D. Wilman,[1] M. Salvato,[1] M. Tanaka,[6] K. Nandra,[1] D. Lutz,[1] D. Elbaz,[7] M. Dickinson,[8] B. Altieri,[9] H. Aussel,[7] S. Berta,[1] A. Cimatti,[10] D. Fadda,[11] R. Genzel,[1] E. Le Floc'h,[7] B. Magnelli,[12] R. Nordon,[13] A. Poglitsch,[1] F. Pozzi,[10] M. Sanchez Portal,[9] L. Tacconi,[1] F. E. Bauer,[14,15] W. N. Brandt,[16] N. Cappelluti,[4,17] M. C. Cooper[18] and J. S. Mulchaey[19]

[1]*Max-Planck-Institut für extraterrestrische Physik, Giessenbachstraße 1, D-85748 Garching bei München, Germany*
[2]*School of Physics and Astronomy, University of Birmingham, Edgbaston, Birmingham B15 2TT, UK*
[3]*Department of Physics, University of Helsinki, Gustaf Hällströmin katu 2a, FI-00014 Helsinki, Finland*
[4]*University of Maryland Baltimore County, 1000 Hilltop circle, Baltimore, MD 21250, USA*
[5]*INAF/Osservatorio Astronomico di Trieste, via G. B. Tiepolo 11, I-34143 Trieste, Italy*
[6] *National Astronomical Observatory of Japan, 2-21-1 Osawa, Mitaka, Tokyo 181-8588, Japan*
[7]*Laboratoire AIM, CEA/DSM-CNRS-Université Paris Diderot, IRFU/Service d'Astrophysique, Bât. 709, CEA-Saclay, F-91191 Gif-sur-Yvette, Cedex, France*
[8]*National Optical Astronomy Observatory, 950 North Cherry Avenue, Tucson, AZ 85719, USA*
[9]*Herschel Science Centre, European Space Astronomy Centre, ESA, Villanueva de la Cañada, E-28691 Madrid, Spain*
[10]*Dipartimento di Astronomia, Università di Bologna, Via Ranzani 1, I-40127 Bologna, Italy*
[11]*NASA Herschel Science Center, Caltech 100-22, Pasadena, CA 91125, USA*
[12]*Argelander-Institut für Astronomie, Universität Bonn, Auf dem Hügel 71, D-53121 Bonn, Germany*
[13]*School of Physics and Astronomy, The Raymond and Beverly Sackler Faculty of Exact Sciences, Tel Aviv University, Tel Aviv 69978, Israel*
[14]*Instituto de Astrofísica, Facultad de Física, Pontificia Universidad Católica de Chile, 306, Santiago 22, Chile*
[15]*Space Science Institute, 4750 Walnut Street, Suite 205, Boulder, CO 80301, USA*
[16]*Department of Astronomy and Astrophysics, 525 Davey Laboratory, The Pennsylvania State University, University Park, PA 16802, USA*
[17]*INAF-Osservatorio Astronomico di Bologna, Via Ranzani 1, I-40127 Bologna, Italy*
[18]*Center for Galaxy Evolution, Department of Physics and Astronomy, University of California, Irvine, 4129 Frederick Reines Hall Irvine, CA 92697, USA*
[19]*The Observatoires of the Carnegie Institution of Science, 813 Santa Barbara Street, Pasadena, CA 91101, USA*

Accepted 2013 October 3. Received 2013 September 22; in original form 2013 April 29

ABSTRACT

We investigate the evolution of the star formation rate (SFR)–density relation in the Extended *Chandra* Deep Field South and the Great Observatories Origin Deep Survey fields up to $z \sim 1.6$. In addition to the 'traditional method', in which the environment is defined according to a statistical measurement of the local galaxy density, we use a 'dynamical' approach, where galaxies are classified according to three different environment regimes: group, 'filament-like' and field. Both methods show no evidence of an SFR–density reversal. Moreover, group galaxies show a mean SFR lower than other environments up to $z \sim 1$, while at earlier epochs group and field galaxies exhibit consistent levels of star formation (SF) activity. We find that processes related to a massive dark matter halo must be dominant in the suppression of the SF below $z \sim 1$, with respect to purely density-related processes. We confirm this finding by studying the distribution of galaxies in different environments with respect to the so-called main sequence (MS) of star-forming galaxies. Galaxies in both group and 'filament-like' environments preferentially lie below the MS up to $z \sim 1$, with group galaxies exhibiting lower levels of star-forming activity at a given mass. At $z > 1$, the star-forming galaxies in groups reside on the MS. Groups exhibit the highest fraction of quiescent galaxies up

⋆ E-mail: fziparo@star.sr.bham.ac.uk

to $z \sim 1$, after which group, 'filament-like' and field environments have a similar mix of galaxy types. We conclude that groups are the most efficient locus for SF quenching. Thus, a fundamental difference exists between bound and unbound objects, or between dark matter haloes of different masses.

Key words: galaxies: evolution – galaxies: groups: general – galaxies: star formation – infrared: galaxies.

1 INTRODUCTION

The properties of galaxies in the local Universe appear to depend strongly on their environment. This issue was highlighted by Dressler (1980) with the so-called morphology–density relation. Namely, massive ellipticals and S0 galaxies are preferentially found in crowded regions, such as cluster cores, while spiral and disc galaxies prefer less dense environments.

It is also well established that a rather tight correlation exists between morphological type and level of star formation (SF) activity. In general, disc galaxies tend to have a higher star formation rate (SFR) than spheroidal systems. Recently, the nature of this relation has been carefully studied up to $z \sim 2.5$ by Wuyts et al. (2011), through the use of the deep *Herschel*[1] surveys and well-calibrated complementary SFR indicators on the major blank fields, such as the Great Observatories Origin Deep Survey (GOODS; Giavalisco et al. 2004) and Cosmological Evolution Survey (COSMOS; Scoville et al. 2007) fields. This work highlights that the so-called main sequence (MS) of star-forming systems, observed at any redshift (e.g. Daddi et al. 2007; Elbaz et al. 2007; Noeske et al. 2007a), corresponds to a well-defined sequence of disc galaxies, while spheroidal systems tend to live below the MS. In light of this finding, the SFR–density relation can be seen as an alternative way to study the morphology–density relation.

A galaxy's SFR is on average anticorrelated with the galaxy density in the local Universe (Lewis et al. 2002; Gómez et al. 2003; Kauffmann et al. 2004). In fact, highly star-forming galaxies are mostly found in low-density environments, while the cores of massive clusters are full of massive, early-type galaxies dominated by old stellar populations. However, the way this relation evolves with redshift is still a matter of debate.

It has been argued that as we approach the epoch at which early-type galaxies form the bulk of their stars at $z \gtrsim 1.5$ (e.g. Rettura et al. 2010), the SFR–density should progressively reverse, such that high-density regions host highly star-forming galaxies at earlier cosmic time. Elbaz et al. (2007) and Cooper et al. (2008) observe this reversal already at $z \sim 1$ in the GOODS field and the DEEP2 Galaxy Redshift Survey, respectively. Using *Herschel* Photodetecting Array Camera and Spectrometer (PACS; Poglitsch et al. 2010) data, Popesso et al. (2011) detect the reversal only for high-mass galaxies. According to the authors, this is due to high-mass galaxies being more likely to host active galactic nuclei (AGN). Since AGN exhibit a slightly higher SFR with respect to galaxies of the same stellar mass (Santini et al. 2012), AGN hosts tend to be star forming (see also Rosario et al. 2013). On the other hand, Feruglio et al. (2010), Ideue et al. (2009, 2012) and Tanaka et al. (2009) find no reversal in the COSMOS field, arguing that the reversal, if any, must occur at $z \sim 2$.

[1] *Herschel* is an ESA space observatory with science instruments provided by European-led Principal Investigator consortia and with important participation from NASA.

The aforementioned studies, use different SFR indicators. Cooper et al. (2008) and Muzzin et al. (2012) convert the [O II] emission line flux into an SFR, while Elbaz et al. (2007), Feruglio et al. (2010) and Tran et al. (2010) use *Spitzer* Multiband Imaging Photometer (MIPS) 24 μm data to measure the SF activity of their galaxy sample. In addition, Elbaz et al. (2007) complement the estimates of SFR derived from the 24 μm flux with those from ultraviolet (UV) emission. All of these estimators can be heavily affected by dust extinction uncertainties, by AGN contamination and/or by metallicity (e.g. Kewley, Geller & Jansen 2004). These problems can be overcome by measuring the SFR from the far-infrared (IR) luminosity, as done in Popesso et al. (2011). Indeed, *Herschel* PACS data cover the wavelength range at which the bulk of the UV light is re-emitted by dust, at least up to $z \sim 1.5$ (Elbaz et al. 2011). This enables an accurate estimate of the SFR and avoids possible contamination by AGN emission, more common in the mid-IR spectral range (Netzer et al. 2007).

Also the definition of the environment estimated via the local galaxy density is somewhat arbitrary. Indeed, several works measure the distance to the *N*th nearest neighbour (e.g. Cooper et al. 2008). This method is strongly dependent on *N*: small values probe high-density regions better though they smooth the low-density ones, while high values of *N* could wash out the information on overdensities when the number of galaxies in a given halo is less than *N* (Cooper et al. 2005; Muldrew et al. 2012; Woo et al. 2013). Other authors measure the density of neighbours within a fixed comoving volume centred on each galaxy (e.g. Elbaz et al. 2007; Popesso et al. 2011).

All of these methods rely on the assumption that the local number density of galaxies is a good representation of the environment. However, if the environment is defined as the halo mass of the parent halo to which the galaxy belongs, this is not necessarily the case. Indeed, a filament (interconnecting 'nodes' of the same large-scale structure), the outskirts of a massive galaxy cluster and the core of a galaxy group could exhibit the same galaxy density, even being sites of quite different physical processes (on multiple scales these environments can be separated; see e.g. Wilman, Zibetti & Budavári 2010).

Further complication is added by the interplay of mass and density. According to Kauffmann et al. (2004), mass and galaxy density are coupled, with the high-mass galaxies segregated in the densest environments. This relation was already in place at $z \sim 1$ (Scodeggio et al. 2009; Bolzonella et al. 2010). Therefore, the evidence for a clear SFR–density trend could be due to a different contribution of massive and less-massive galaxies favouring different density regimes.

In order to shed light on the relation between SFR, density and halo mass, we take advantage of the combination of the deepest available *Spitzer* and *Herschel* surveys of the Extended *Chandra* Deep Field South (ECDFS) and the GOODS-South and -North fields (GOODS-S and GOODS-N, respectively), observed in the PACS Evolutionary Probe (Lutz et al. 2010) and GOODS-*Herschel* (Elbaz et al. 2011) surveys. The combined GOODS data from these

two surveys are described in Magnelli et al. (2013). In this work, we use a spectroscopic selected sample as already done in Ziparo et al. (2013, Z13 hereafter).

We first study the SFR–density relation up to $z \sim 1.6$ in its standard definition, by estimating the local galaxy density parameter. In the second part of the paper, we propose an alternative definition of the SFR–environment relation: we distinguish between galaxy group members, 'filament-like' environments and galaxies that are isolated or more likely associated with lower mass haloes. For this analysis, we use the galaxy group sample studied in Z13. In addition, we try to break the mass–density (environment) degeneracy, by studying the location of group galaxies in the SFR–M_* (M_*) plane as a function of environment up to $z \sim 1.6$.

This paper is organized as follows: in Section 2, we briefly describe our data set and analysis. In Section 3, we present our results and we discuss them in Section 4. Eventually, we draw our conclusions in Section 5. Throughout our analysis we adopt a Chabrier (2003) initial mass function and the following cosmological parameters: $H_0 = 70\,km\,s^{-1}\,Mpc^{-1}$, $\Omega_M = 0.3$ and $\Omega_\Lambda = 0.7$.

2 THE DATA SET

In Z13, we create a clean Infrared Array Camera (IRAC; Fazio et al. 2004) 3.6 μm selected galaxy sample in the ECDFS and GOODS fields. This sample includes only galaxies with a spectroscopic redshift and is drawn from the galaxy catalogues of Cardamone et al. (2010), Grazian et al. (2006) and Wuyts et al. (2011), in the ECDFS, the GOODS-S and the GOODS-N field, respectively. The group sample studied in Z13 also includes the X-ray groups identified in the COSMOS field by Finoguenov et al. (2007), George et al. (2011) and George et al. (2012), and employs the group membership defined by Popesso et al. (2012). However, given the rather low spectroscopic completeness in the COSMOS field (40 per cent in the M_* range of interest, see Z13 for a complete discussion), this region is not included in our current analysis. Indeed, it is not possible to reliably estimate the local galaxy density parameter on the basis of the pure spectroscopic data. The use of both spectroscopic and photometric redshifts, as done in Kovač et al. (2010), is preferable in the COSMOS field, where the sampling rate is spatially very inhomogeneous. Thus, since the ECDFS and the GOODS fields show an extremely high spectroscopic completeness (60–80 per cent in M_*), we prefer to restrict our analysis to these regions.

We measure the SFR by using the deepest available *Spitzer* MIPS 24 μm data combined with the deepest *Herschel* PACS 100 and 160 μm data. In order to overcome any blending issue, the *Spitzer* and *Herschel* flux densities are derived with a point-spread-function-fitting analysis guided by the position of sources detected in deep IRAC images (see Magnelli et al. 2011, 2013). This method solves a large part of the blending issues encountered (see results of dedicated Monte Carlo simulations in Magnelli et al. 2013) and provides a straightforward association between IRAC, MIPS and PACS sources. Furthermore, even if in high-density regions the prior PSF-fitting method does not solve all blending issues, it should still provide reliable estimates of the total IR fluxes of these clustered regions and, thus, of their total SFR activity.

The SFR is estimated with the use of the IR templates of Elbaz et al. (2011). For sources undetected in PACS and with only MIPS detections, we use the 'MS' template, which turns out to provide the most accurate estimate of the SFR from mid-IR data. In order to complement the SFR derived from IR data (available for the bulk of the star-forming population) with the SFR of the low star forming or rather inactive galaxies (i.e. undetected in the mid- and far-IR surveys), we measure the SFR via multiwavelength spectral energy distribution (SED) fitting by using PHotometric Analysis for Redshift Estimations[2] (*Le PHARE*; Arnouts et al. 2001; Ilbert et al. 2006) and the Bruzual & Charlot (2003) library. For this purpose, we use the aforementioned multiwavelength photometric catalogues (Grazian et al. 2006; Cardamone et al. 2010; Wuyts et al. 2011).

Z13 provide a careful calibration of the SFR derived via SED fitting with respect to the more reliable SFR derived from IR data. We find consistent estimates of SFR though the scatter is quite large, ranging from 0.5 to 0.7 dex depending on the redshift range.

The SED fitting technique is also useful for estimating stellar masses. The comparison of our estimates with those derived from the same catalogues via different methods and/or templates shows that we can accurately estimate M_* within a factor of 2 (see Z13 for more details).

The spectroscopic data used for the construction of the density field and the dynamical analysis of the galaxy group sample are taken from a collection of publicly available high-quality spectroscopic redshifts in the ECDFS (Popesso et al. 2009; Balestra et al. 2010; Cardamone et al. 2010; Silverman et al. 2010; Cooper et al. 2012, see Z13 for further details about the combination of the different catalogues). The spectroscopic catalogue of the GOODS-N field is taken from Barger, Cowie & Wang (2008).

2.1 The galaxy group sample and their members

All the blank fields considered in our analysis are observed extensively in the X-ray with *Chandra* and *XMM–Newton*. The X-ray data reduction and the creation of the X-ray group catalogues are explained in detail in Finoguenov et al. (2009) and in Finoguenov et al. (in preparation). As explained in Z13, we select a subsample of X-ray selected groups with clear optical (spectroscopic) identification (we do not include groups with more than one redshift peak of similar strength along the line of sight), without close companions that might affect the membership determination, and with at least 10 members, to reliably estimate the velocity dispersion and the membership. This selection leads to a sample of 22 X-ray detected groups in the ECDFS and 2 groups in the GOODS-N field. We also consider a large-scale structure spectroscopically confirmed at $z \sim 1.6$ by Kurk et al. (2009).

Fig. 1 shows the group mass[3] estimates as a function of redshift for the ECDFS (in blue) and GOODS (in red) fields, respectively. We also show the dynamical mass estimates for the groups in the GOODS fields from Popesso et al. (2012). The dynamical analysis of each structure is based on spectroscopic data. For details on the dynamical analysis and group membership, see Popesso et al. (2012) and Z13.

In order to follow the evolution of the relation between SFR and environment, we divide our galaxy sample into four redshift bins, $0 < z \leq 0.4$, $0.4 < z \leq 0.8$, $0.8 < z \leq 1.2$ and $1.2 < z \leq 1.7$, according to the redshift distribution of our group sample. We note that the last redshift bin is populated only by the structure at $z \sim 1.6$ (Kurk et al. 2009). This is a likely supergroup or a cluster in formation as suggested by the X-ray emission from different extended sources in the structure (Finoguenov et al. in preparation). When

[2] http://www.cfht.hawaii.edu/~arnouts/LEPHARE/cfht_lephare/lephare.html

[3] M_Δ (where $\Delta = 500, 200$) is defined as $M_\Delta = (4\pi/3)\Delta\rho_c R_\Delta^3$, where R_Δ is the radius at which the density of a cluster is equal to Δ times the critical density of the Universe (ρ_c).

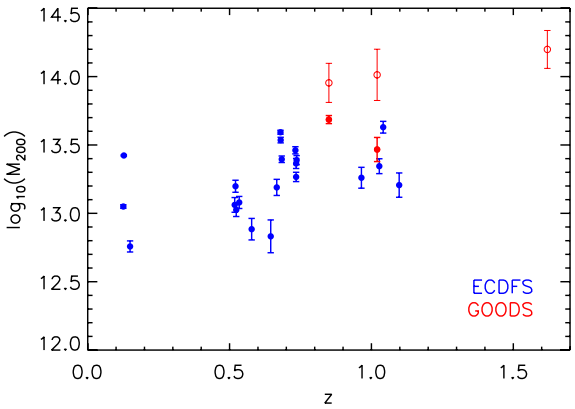

Figure 1. M_{200} as a function of redshift for all groups considered in our sample. The filled circles represent the X-ray mass estimates, while empty circles show the dynamical mass estimates. We highlight in blue the ECDFS sample and in red the GOODS groups.

we analyse the SFR–environment relation by distinguishing group members from systems in other environments, we consider, in each redshift bin, all group galaxies together as members of a composite group. This is done to increase the statistics of group galaxies which otherwise would be too low when considering individual systems.

To limit the selection effects and at the same time to control the different levels of spectroscopic completeness in different redshift bins (see e.g. fig. 5 in Z13), we apply a common stellar mass cut at $M_* = 10^{10.3}\,\mathrm{M}_\odot$. This mass cut corresponds to an IRAC 3.6 μm apparent magnitude brighter than the 5σ detection limit in each considered field up to $z \sim 1.7$, enabling a high spectroscopic completeness. Moreover, the considered mass range is still dominated by sources with MIPS and/or PACS detections, in other words with robust SFR estimates. The uncertainties due to the spectroscopic incompleteness of our galaxy sample are evaluated with dedicated Monte Carlo simulations based on the mock catalogues of Kitzbichler & White (2007) drawn from the Millennium simulation (Springel et al. 2005).

2.2 The local galaxy density

The key ingredient for building a reliable density field is very high and spatially uniform spectroscopic coverage. This is reached in the ECDFS (see Cooper et al. 2012) and in the GOODS fields (see Elbaz et al. 2007; Popesso et al. 2011), for which we reconstruct the density around each galaxy up to $z \sim 1.7$.

We use a method similar to Popesso et al. (2011) to compute the projected local galaxy density, Σ, around each spectroscopically confirmed galaxy with $M_* > 10^{10.3}\,\mathrm{M}_\odot$. We count all galaxies located inside a cylinder of radius 0.75 Mpc, within a fixed velocity interval around each galaxy of $\Delta v = 3000\,\mathrm{km\,s^{-1}}$, about 10 times the typical velocity dispersion of galaxy groups ($\sigma_v \sim 300$–$500\,\mathrm{km\,s^{-1}}$), and above a redshift dependent mass limit [$M_{\mathrm{cut}}(z)$]. Given the spectroscopic completeness as a function of M_* in the four redshift bins considered in our analysis (see Z13), we choose as a cut the M_* value where the 40–50 per cent completeness limit is reached in each redshift bin: $M_*/\mathrm{M}_\odot = 10^9$ at $0 < z < 0.4$, $M_*/\mathrm{M}_\odot = 10^{9.5}$ at $0.4 < z < 0.8$, $M_*/\mathrm{M}_\odot = 10^{10}$ at $0.8 < z < 1.2$ and $M_*/\mathrm{M}_\odot = 10^{10.3}$ at $1.2 < z < 1.7$. This does not lead to a different density field definition as a function of redshift bin, but only to a more robust density estimate in the bins where the spectroscopic completeness is still very high at low masses. Indeed, only the absolute value of the density parameter changes, but the relative difference between high- and low-density regions is kept the same with respect to the choice of a fixed $M_* = 10^{10.3}\,\mathrm{M}_\odot$ at any redshift.

The density field obtained with the chosen $M_{\mathrm{cut}}(z)$, rather than that at a fixed mass cut of $M_* = 10^{10.3}\,\mathrm{M}_\odot$, allows us to distinguish between galaxies residing in dark matter haloes of different masses. However, the density fields obtained with a lower mass cut show, as expected, higher values and a slightly higher accuracy in distinguishing between galaxies located in parent haloes of different masses. We estimate that, on average, the projected density obtained with a mass cut of $M_*/\mathrm{M}_\odot = 10^9$ at $0 < z < 0.4$ is a factor of 7 higher than that at $M_*/\mathrm{M}_\odot = 10^{10.3}$. At $0.4 < z < 0.8$, a mass cut of $M_*/\mathrm{M}_\odot = 10^{9.5}$ leads to a density a factor of 5 higher than the cut at lower M_*, while at $0.8 < z < 1.2$ the density with a mass cut of $M_*/\mathrm{M}_\odot = 10^{10}$ is a factor of 2.5 higher. These calibrations are discussed in depth in a dedicated forthcoming paper (Popesso et al., in preparation).

A more physical definition of the density field would require a mass cut which takes into account the evolution of the characteristic magnitude of the stellar mass function. In our case, this would translate to selecting only galaxies at masses larger than M^* at any redshift (Ilbert et al. 2010), given the restriction imposed by the completeness level of the galaxy sample in the higher redshift bins. This would imply that at lower redshifts we would select only galaxies with $M_* > 10^{11}\,\mathrm{M}_\odot$, limiting in a significant way the statistics for defining the density field. Thus, distinguishing between galaxies residing in parent haloes of different masses would be inefficient. A simple exercise on the mock catalogues of Kitzbichler & White (2007) reveals that this density definition would be able to distinguish only isolated galaxies from galaxies in the core of massive clusters and it would provide the same density for galaxies in haloes with masses ranging from 10^{12} to $10^{14.5}\,\mathrm{M}_\odot$.

In order to consider the effect of spectroscopic incompleteness, we correct the density Σ by accounting for the possibly missing galaxies. We consider, for each galaxy, the cylinder along the line of sight, with radius of 0.75 Mpc at the redshift of the considered source, and with redshift limits z_{min} and z_{max} equal to the limits of the redshift bin to which the source belongs. The spectroscopic completeness is given by the number of sources with spectroscopic redshifts divided by the total number of galaxies, considering only sources with $M_* > M_{\mathrm{cut}}(z)$. Since the redshift bins are more than 10 times larger than the error on the photometric redshift, this uncertainty is only marginally affecting our completeness estimate. We correct for incompleteness by dividing Σ by this ratio.

In order to test the reliability of our density estimate, we measure, with the same method, the density field in 100 randomly extracted catalogues from the mock catalogues of Kitzbichler & White (2007). We compare the density obtained in this way with that measured in the parent light-cone mock catalogues, free of selection biases. In order to simulate the photometric redshift uncertainty, before estimating the incompleteness correction, we assign a random error in the range $-\Delta z < \delta z_{\mathrm{phot}} < \Delta z$ to the redshift of the parent mock catalogue galaxies, where Δz is the photometric redshift error provided in the photometric catalogues. We find a very good agreement between the original density estimated in the Kitzbichler & White (2007) mock catalogues and the local density retrieved with our method (Fig. 2). We also use this approach for estimating the error per density bin as the dispersion of $\Sigma_{\mathrm{original}} - \Sigma_{\mathrm{retrieved}}$.

Our density definition takes advantage of the high level of mass segregation observed in the local Universe (Kauffmann et al. 2004) and at least up to $z \sim 1$. Since we estimate the density of rather

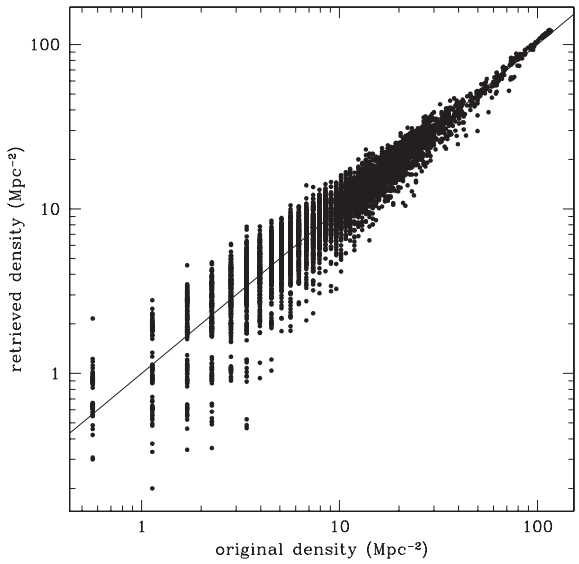

Figure 2. Comparison between the original local density estimated in the Kitzbichler & White (2007) mock catalogues and the density retrieved in the randomly extracted catalogue following our method. The solid line shows the one-to-one relation.

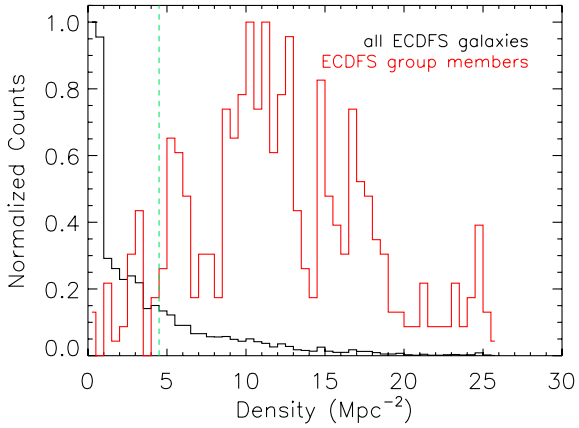

Figure 3. In black: density distribution around each galaxy with a spectroscopic redshift in ECDFS. The red histogram shows the density of group members. The green dashed line at 4.5 galaxies Mpc^{-2} nicely separates the group-dominant regime from the field-dominant regime. Indeed, 75 per cent of field galaxies are found at densities below this threshold and 92 per cent of group galaxies above that.

massive galaxies around each system, our density estimator should be able to better distinguish between high-density regions, generally dominated by massive galaxies, from low-density regions, more populated by low-mass systems. Indeed, Fig. 3 shows that our method is able to nicely isolate galaxies identified as group spectroscopic members (red histogram) from isolated galaxies (the peak below $\Sigma \sim 3$–$4\,\mathrm{Mpc}^{-2}$). A similar figure is shown in Cooper et al. (2012, their fig. 11) based on the third-nearest-neighbour density estimator. The comparison of the two figures shows that our density estimator is more efficient in distinguishing isolated systems from galaxy group members. In fact, although groups occupy the highest density bins in Cooper et al. (2012, their fig. 11), they are not clearly isolated from field galaxies as in our case.

3 RESULTS

We first build the SFR–density relation by studying the statistical correlation between the SFR and density parameters, as usually done in the literature. This lets us compare our results with previous works. As a second approach, we use a dynamical definition of environment by differentiating among massive bound structures, less-massive bound or unbound structures and relatively isolated galaxies. We follow the evolution of the relation in both cases up to $z \approx 1.6$ and we test and compare our results with the predictions of simulations.

3.1 The 'environmental' approach

Fig. 4 shows the SFR–density relation for all galaxies with $M_* > 10^{10.3}\,\mathrm{M}_\odot$ in four redshift bins. The errors in Fig. 4 are derived from our error analysis using the mock catalogues of Kitzbichler & White (2007), as explained in Section 3.1.1. We find a significant anticorrelation up to $z \sim 0.8$, confirmed by the Spearman test at 3σ confidence level. At $0.8 < z < 1.2$ we find an anticorrelation but with lower significance (2.3σ). In the highest redshift bin, comprising the Kurk et al. (2009) large-scale structure, we do not find any significant anticorrelation ($<2\sigma$ significance level). Thus, we can exclude with high confidence level (from the Spearman test) any positive correlation in the last two redshift bins as claimed in previous works (e.g. Elbaz et al. 2007; Cooper et al. 2008). We only observe a progressive flattening towards higher redshifts, but no reversal of the relation.

The shapes of the relations shown in Fig. 4 are noisy and not even linear in log–log space. Thus, it cannot be easily fitted by a simple fitting function. In order to quantify the steepness of the relation, we simply estimate the ratio between the mean SFR at densities below and above the median local galaxy density Σ. Below $z \sim 1.2$, where we see an anticorrelation, although with different significances depending on the redshift bin, the mean SFR in low-density regions spans a range of 1.4–2.1 times the mean SFR in high-density regions. In the highest redshift bin, we do not observe a significant difference between the SFR in low- and high-density regions.

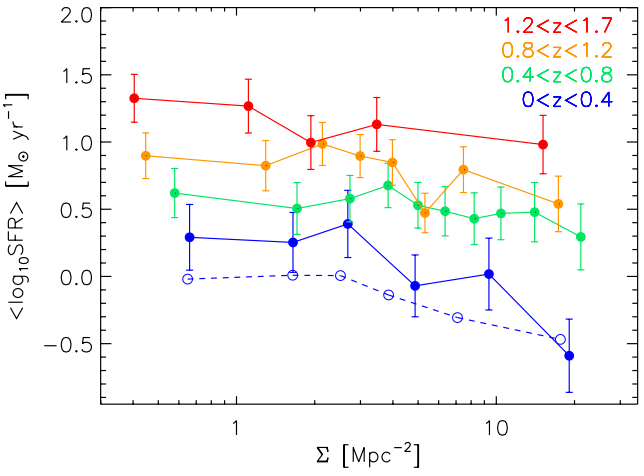

Figure 4. SFR–density relation for galaxies with $M_* > 10^{10.3}\,\mathrm{M}_\odot$ in different redshift bins (solid lines). The dashed line represents the SFR–density relation at $0 < z < 0.4$ for all galaxies with $M_* > 10^9\,\mathrm{M}_\odot$. Errors are derived using the mock catalogues of Kitzbichler & White (2007), as explained in the text.

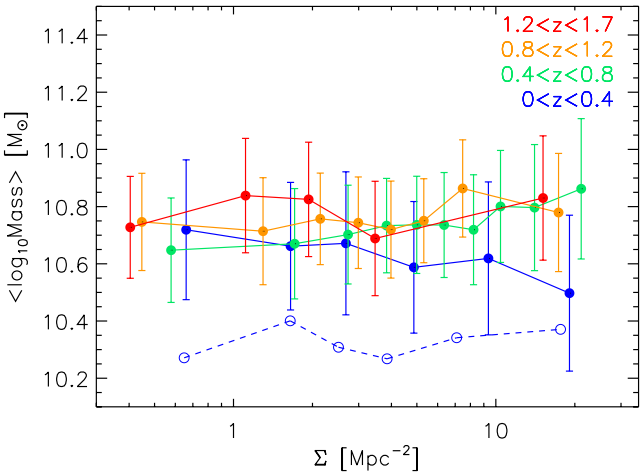

Figure 5. Stellar mass–density relation for all the galaxies with $M_* > 10^{10.3}\,M_\odot$ in different redshift bins (solid lines). Errors are derived using the mock catalogues of Kitzbichler & White (2007), as explained in the text. The dashed line represents the M_*–density relation at $0 < z < 0.4$ for all galaxies with $M_* > 10^9\,M_\odot$. The normalization of the dashed line is artificially increased to higher value to make it close to the blue solid line and make the comparison easier.

What is the role of group galaxies in shaping the relations? In order to check this, we remove from the sample all galaxies dynamically associated with either extended X-ray-emitting sources or the structure at $z \sim 1.6$. We also remove all galaxies associated with extended X-ray-emitting sources not included in the final group sample. In the two lowest redshift bins, the significance of the anticorrelation decreases much below the 3σ level. In the highest two redshift bins, we exclude both a reversal and any sign of anticorrelation. This clearly shows the dominant role of group environments in shaping the SFR–density anticorrelation observed in the local Universe and at intermediate redshift.

In principle, a prominent mass segregation together with a high fraction of low-star-forming galaxies (typical of the group and cluster environment) could easily lead to the SFR–density anticorrelation observed at low and intermediate redshift. Fig. 5 shows the M_*–density relation for the same sample of galaxies in the four redshift bins. We do not measure a strong mass segregation in the galaxy sample used for the SFR–density relation analysis. The first redshift bin exhibits a slightly different behaviour with respect to the relation in the other redshift bins. However, given the large errors (for their computation see Section 3.1.1), we cannot draw a definitive conclusion on the M_*–density trend. The Spearman test confirms only a mild level of mass segregation at $0.4 < z < 0.8$. Thus, the SFR–density anticorrelation observed in the first and second redshift bins is not caused by mass segregation.

In the local Universe, mass segregation is observed with high significance by Kauffmann et al. (2004) on the basis of a large sample of Sloan Digital Sky Survey (SDSS; York et al. 2000) galaxies. Are our results at odds with previous findings? The main difference with respect to Kauffmann et al. (2004) is the mass cut applied to our sample. Indeed, for spectroscopic completeness issues, we are considering only massive galaxies, i.e. with $M_* > 10^{10.3}\,M_\odot$. The dashed blue line in Fig. 5 shows the mass–density relation obtained after applying a mass cut of $10^9\,M_\odot$ in the lowest redshift bin. This analysis is possible without strong biases only at low redshift where the spectroscopic completeness is rather high even at low stellar masses (see Z13). The Spearman test reveals a mild positive correlation. The absence of a stronger correlation, as found e.g. in Kauffmann et al. (2004), could be due to the lack of many massive spectroscopically detected galaxies at low redshift (see fig. 5 of Z13), since in ECDFS this type of galaxies was targeted for spectroscopy only at high redshift (e.g. Popesso et al. 2009). We point out that we observe an even more significant (according to the Spearman test) SFR–density anticorrelation (blue dashed line in Fig. 4) in the lowest redshift bin after applying the lower mass cut. This probably indicates that, in a broader mass regime, mass segregation enhances the significance of the SFR–density relation in the parent sample.

3.1.1 How robust is our analysis of the SFR–density relation?

In order to take into account all possible biases inherent in our spectroscopic selection, we study the SFR–density relation in a simulated Universe. We analyse the SFR–density relation obtained using the Kitzbichler & White (2007) mock catalogues (five different light cones) by applying our definition of local galaxy density. We observe an anticorrelation in all redshift bins (5σ significance). Thus, our results (Fig. 4) are at least qualitatively in agreement with the prediction of Kitzbichler & White (2007), except in the highest redshift bin. However, we point out that the SFR–density relations measured using the mock catalogues are observed in an area of sky that is a magnitude larger than the ECDFS and the GOODS-N regions. Thus, the mock catalogues sample a much broader range of densities due to the presence of massive clusters, while our data set comprises only groups.

In order to check the effect of cosmic variance when using a rather small area, we estimate the SFR–density relation in 1000 different regions of the Kitzbichler & White (2007) light cones with areas similar to the sum of the ECDFS and GOODS-N areas. After running a Spearman test, we detect an anticorrelation with at least 3σ significance in all regions in the two redshifts bins below $z \sim 0.8$. At $0.8 < z < 1.2$, we measure an anticorrelation in 98 per cent of the cases and at higher redshift in 70 per cent of the cases. The non-correlation in the observed $1.2 < z < 1.7$ redshift bin could be due to the low probability of finding massive large-scale structures in such a small area and at high redshift in the Λ cold dark matter (ΛCDM) cosmology. It could also be due to larger errors on environment washing out the signal (see e.g. Cooper et al. 2010). Thus, cosmic variance could considerably affect the significance of an anticorrelation.

In order to simulate the spectroscopic completeness in the ECDFS and GOODS regions, we randomly extract a subsample of galaxies from the Millennium mock catalogues mimicking the spectroscopic completeness of the observed data. We extract randomly a percentage of galaxies consistent with the spectroscopic completeness in one of the available photometric bands and for each magnitude bin of our galaxy sample. This procedure randomly extracts 100 different catalogues that nicely reproduce the selection function of our sample (see Z13 for further details). We point out that while the galaxy mock catalogues of the Millennium simulation provide a rather good representation of the local Universe, at higher redshifts ($z > 1$) they fail to reproduce the correct distribution of star-forming galaxies in the SFR–M_* plane. Indeed, Elbaz et al. (2007) find that at $0.8 < z < 1.2$ the galaxy SFR is underestimated, on average, by a factor of 2, at fixed M_*, with respect to the observed values. By performing the same exercise with our data set, we find that this underestimate ranges by factors of 2.5 to 3 at $1.2 < z < 1.7$. However, this does not represent a problem with our approach. Indeed, the aim of this analysis is to understand what is the bias introduced

by a selection function similar 'in relative terms' to the spectroscopic selection function of our data set. Thus, for our needs, it is sufficient that the randomly extracted mock catalogues reproduce the same bias in selecting, on average, the same percentage of most star forming and most massive galaxies of the parent sample, as shown in Z13. The bias of our analysis is estimated by comparing the results obtained with and without our galaxy sampling. Since the underestimate of the SFR or the M_* of high-redshift galaxies is common to both, biased and unbiased, samples, it does not affect the result of this comparative analysis. We also stress that the aim of this analysis is not to provide correction factors for our observational results but a way to interpret our results taking into account possible biases introduced by the spectroscopic selection function.

In order to account for both the spectroscopic completeness and the cosmic variance, we repeat the exercise performed with the complete Kitzbichler & White (2007) mock catalogues by extracting 1000 different regions with areas similar to the sum of the ECDFS and GOODS-N areas in the incomplete mock catalogues. We estimate the SFR–density relation in each region as done on the real data set. The probability of non-correlation increases to ∼5 per cent in lower redshift bins, 12 per cent at $0.8 < z < 1.2$ and 45 per cent at $1.2 < z < 1.7$. This suggests that small areas (thus cosmic variance), in addition to spectroscopic incompleteness, could hide a possible anticorrelation in the highest redshift bin or reduce the significance of the anticorrelation in the lower redshift bins.

This last exercise allows us to quantify the possible bias in the estimate of the SFR–density relation due to our spectroscopic selection. We measure the mean SFR by using the same binning in density in the incomplete and in the original complete catalogues. In this way, we can compute the residual $\Delta\mathrm{SFR}(\Sigma) = \langle\mathrm{SFR}_{\mathrm{observed}}(\Sigma)\rangle / \langle\mathrm{SFR}_{\mathrm{true}}(\Sigma)\rangle$, where $\langle\mathrm{SFR}_{\mathrm{observed}}\rangle$ is the mean SFR estimated in the incomplete catalogue at the given density bin, and $\langle\mathrm{SFR}_{\mathrm{true}}\rangle$ is the mean SFR estimated in the complete Kitzbichler & White (2007) mock catalogues at the same density bin. We estimate $\Delta\mathrm{SFR}(\Sigma)$ in 1000 sky regions, extracted from five light cones, with the area similar to the sum of the ECDFS and GOODS-N area, as explained above. We estimate the mean and the dispersion of the $\Delta\mathrm{SFR}(\Sigma)$ distribution in each density bin. The mean indicates whether there is any bias in the spectroscopic selection that leads to an over- or underestimate of the mean SFR per density bin. The dispersion provides the error on the mean SFR per bin.

As shown in Fig. 6, the $\langle\mathrm{SFR}\rangle$ derived from the incomplete mock catalogues is on average a factor of 2–4 (depending on the redshift bin) larger than the 'true' one obtained from the complete Kitzbichler & White (2007) mock catalogues. Thus, the incompleteness leads to a large overestimate of the mean SFR in each density bin. This is easily understandable, since the simulated spectroscopic selection favours highly star-forming galaxies (see Z13). However, the ratio of the observed and true mean SFR is constant as a function of local galaxy density and is of the same order at any redshift. This implies that using our data set we are likely overestimating the mean observed SFR in the same way at any density without biasing the slope of the relation. Thus, our estimate of the SFR–density relation is rather robust despite the spectroscopic incompleteness. We use the dispersion estimated with this procedure to define the errors on the observed SFR–density relation at the corresponding density. This is possible because we find a correspondence between galaxy density field and galaxy parent halo mass both in the observed and simulated data sets, at least in the group regime.

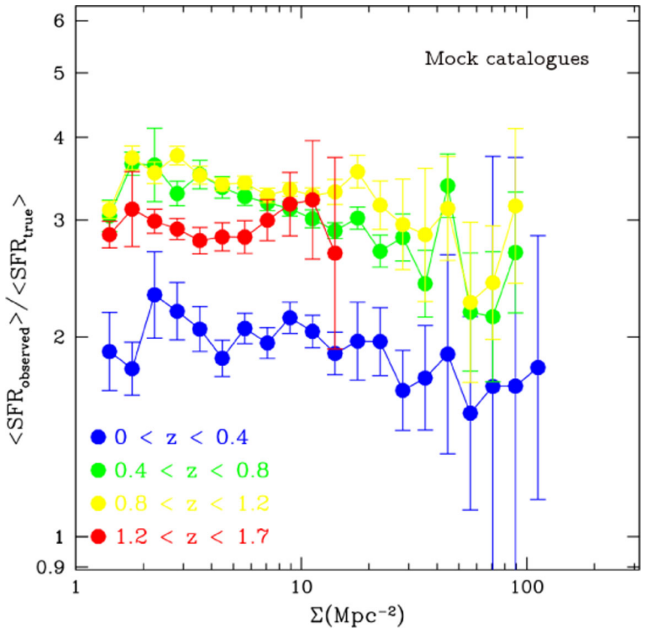

Figure 6. Ratio between the SFR derived from the incomplete mock catalogues ($\langle\mathrm{SFR}_{\mathrm{observed}}\rangle$) and the SFR from the complete ones ($\langle\mathrm{SFR}_{\mathrm{true}}\rangle$) versus density for all four redshift bins used in this work. We do not find any bias in the slope of the SFR–density relation of Fig. 4 as confirmed by the Spearman test.

3.2 Is the SFR–density relation reversing at $z \sim 1$?

The final point of our environmental approach focuses on understanding the disagreement between our findings and previous works claiming a reversal of the SFR–density relation at $z \sim 1$. The fairest comparison is with Elbaz et al. (2007) and Popesso et al. (2011), since our data set includes the sky regions covered by their data set.

Fig. 7 shows the SFR–density relation at $0.8 < z < 1.2$ for the ECDFS and GOODS-N regions separately. In the GOODS-N region, we observe an anticorrelation between SFR and density with high significance, as confirmed by the Spearman test. We do not observe any relation between SFR and density in the ECDFS region

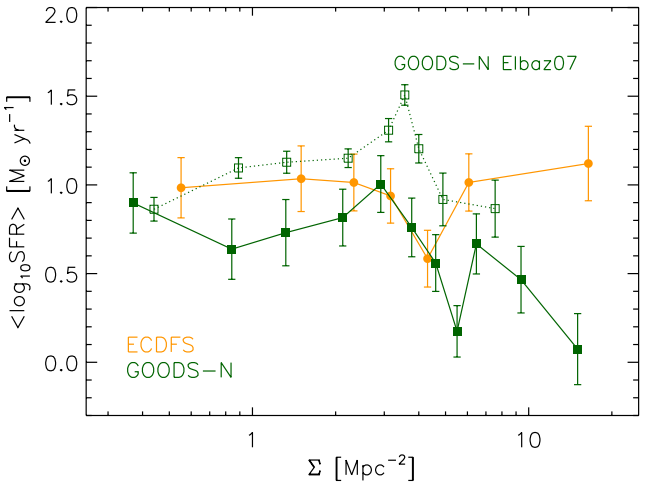

Figure 7. SFR–density relation for all galaxies with $M_* > 10^{10.3}\,\mathrm{M}_\odot$ at $z \sim 1$. Galaxies in the ECDFS and GOODS-N fields are shown in orange and green, respectively. The open symbols connected by a dotted line show the SFR–density relation of Elbaz et al. (2007) for GOODS-North.

which contains only a very poor group at $z = 0.96$, differently from the GOODS-N region that comprises, in the same redshift bin, two very massive groups ($M_{200} \sim 9 \times 10^{13}\,M_{\odot}$). Errors are estimated as in Section 3.1.1.

Fig. 7 also shows the relation of Elbaz et al. (2007) for the GOODS-N region with open symbols connected by a dotted line. We can compare our results with Elbaz et al. (2007) only qualitatively, since the definitions of the density parameter and of the galaxy sample differ considerably. In fact, Elbaz et al. (2007) include all galaxies with *Hubble Space Telescope* ACS $z_{AB} < 23.5$ mag without any mass cut. Given the broad redshift range considered ($0.8 < z < 1.2$), this apparent magnitude cut corresponds to a difference of 0.75 mag from the lowest to the highest redshift limit, introducing a bias with respect to our physical stellar mass selection (see also Cooper et al. 2010). This could explain the offset between our SFR–density relation and that of Elbaz et al. (2007). Elbaz et al. (2007) find a positive correlation in GOODS-N up to the point in which the SFR reaches its maximum and then a rapid decline at higher density. They refer to this as a 'reversal' of the SFR–density relation. Even if we do not detect any reversal, we point out that the trend we observe for the GOODS-N field has a shape similar to that of Elbaz et al. (2011).

The analysis of the SFR–density relation of Elbaz et al. (2007) is based on the estimate of the mean SFR per density bin, rather than on statistical tests such as the Spearman test used in this work. In addition, the errors estimated in Elbaz et al. (2007) seem to be underestimated with respect to ours. Indeed, Elbaz et al. (2007) use a bootstrap technique that cannot take into consideration the effect of cosmic variance due to the relatively small fields considered in the analysis.

Popesso et al. (2011) show that the use of PACS data provides a big advantage (with respect to the MIPS data) in measuring the unbiased SFR of AGN hosts, whose SFR could be enhanced with respect to non-active galaxies of similar M_*. Thus, given the high fraction of AGN (17 per cent) measured at least in the highly star-forming population of the GOODS-S and GOODS-N fields, Popesso et al. (2011) conclude that the reversal of the SFR observed by Elbaz et al. (2007) could be due to a bias introduced by the SFR of AGN host galaxies measured with MIPS data.

In building the SFR–density relation, we are including all galaxies above $10^{10.3}\,M_{\odot}$ with SFR much below the luminous infrared galaxy (LIRG) limit used by Popesso et al. (2011). Taking advantage of the AGN sample of Shao et al. (2010) for the GOODS-N region and the AGN sample of Lutz et al. (2010) for the ECDFS, constructed with similar criteria and X-ray flux limits, we investigate whether AGN can bias our sample. We observe an AGN fraction of 3–5 per cent in the ECDFS and GOODS-N region above our mass cut. This fraction is much lower with respect to the work of Popesso et al. (2011), who show that the fraction of AGN is much higher in highly IR luminous galaxies. Since we include galaxies spanning a wide range in SFR, the AGN fraction is diluted in our sample. If we remove the AGN from our sample, the significance of the SFR–density relation does not change at all, in agreement with Elbaz et al. (2011).

We conclude that the previously observed reversal of the SFR–density relation at $z \sim 1$ is most likely due to a combination of different effects: the galaxy sample selection, a rather high fraction of AGN in the selected sample and a possibly biased definition of the density parameter, which can hide a redshift dependence. In addition, we point out that the significance of this reversal is probably due to an underestimate of the error on the mean SFR, since the cosmic variance is neglected.

3.3 The 'dynamical' approach

As shown in Fig. 3, on the right of the dashed green line, where ∼90 per cent of group galaxies are located, there are still a large number of galaxies at densities comparable to groups but not associated with any extended emitting source identified by the X-ray catalogue of Finoguenov et al. (in preparation). Those galaxies are likely located in unbound large-scale structures, such as filaments, or in dark matter haloes of lower mass with respect to the detection limits of the *Chandra* Deep Field South 4 Ms (Xue et al. 2011).

If the relative vicinity to other galaxies is the main driver in quenching the galaxy SF, we should not observe any difference in the level of SF activity between galaxies showing the same local galaxy density. If, instead, processes related to the dark matter halo play a stronger role, we should observe a difference in the level of SF activity between group galaxies and systems at high density but not related to massive dark matter haloes.

To check this issue, we investigate the SFR–density relation with a novel 'dynamical' approach. We distinguish between galaxies in three different environments: (a) group members, as identified via dynamical analysis, (b) 'filament-like' galaxies identified as systems at the same density as group galaxies but not associated with any of the extended X-ray sources or to the Kurk et al. (2009) structure and (c) isolated galaxies with local galaxy density $\Sigma < 4.5$ Mpc^{-1} (on the left-hand side of the green line of Fig. 3), i.e. where we find a low fraction of group galaxies (8 per cent). We build a new version of the SFR–density relation by comparing the mean SFR in the three environments for all galaxies with $M_* > 10^{10.3}\,M_{\odot}$. This method allows us to isolate the contribution of groups with halo mass $10^{13} \lesssim M_{200}/M_{\odot} \lesssim 2 \times 10^{14}$ in the SFR–density relation.

The left-hand panel of Fig. 8 shows the SFR–density relation according to our new definition. We see a strong evolution with redshift of the mean SFR in groups (within $2 \times R_{200}$) with respect to the other two environments. Indeed, as shown in the right-hand panel of Fig. 8, the ratio of ⟨SFR⟩ is strongly evolving and it shows that the higher the redshift the lower the difference between the level of SF activity in groups and that in the field. This is consistent with the significance of the SFR–density (in its standard definition) anticorrelation decreasing with redshift (see Section 3.1). The right-hand panel of Fig. 8 also shows the ratio between ⟨SFR⟩ of groups and 'filament-like' galaxies. Although the errors are large, it is possible to appreciate how the ratio increases with redshift, with the SF activity of group galaxies being twice that of 'filament-like' galaxies at $z \sim 1.6$. If this trend were real, the structure at $z \sim 1.6$ would provide some hints of the enhancement of the SF activity in groups with respect to filaments. However, since the errors are quite large we cannot draw any definitive conclusion.

The evolution of the SF activity in different environments allows us to better understand the traditional SFR–density relation. In fact, the mix of galaxies in different environments, but at the same densities, hides the strong evolution observed in the left-hand panel of Fig. 8. Our results also suggest that quenching processes related to a massive dark matter halo must play a decisive role in the strong evolution of the SF activity of group members with respect to galaxies in other environments.

We also check if the strong evolution of the newly defined SFR–density relation depends on a similar evolution of the M_*–density relation, using the same approach. Fig. 9 shows the M_*–density relation in the usual four redshift bins according to our novel dynamical definition. The large errors do not allow us to see any strong mass segregation. As in Fig. 5, the lowest redshift bin exhibits a different behaviour with respect to the relation at higher redshifts.

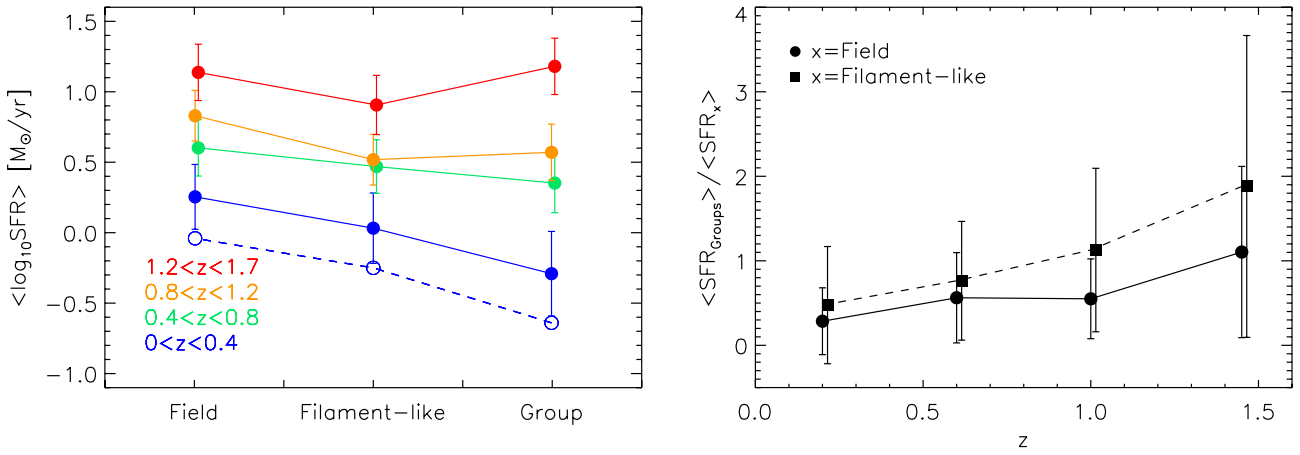

Figure 8. Left: comparison of mean SFR among group (within $2 \times R_{200}$), 'filament-like' and field galaxies. Errors are derived using the mock catalogues of Kitzbichler & White (2007), as explained in the text. The dashed line represents the mean SFR for the different environments at $0 < z < 0.4$ for all galaxies with $M_* > 10^9\,M_\odot$. Right: ratio between the $\langle SFR \rangle$ of group galaxies with respect to field and 'filament-like' galaxies as a function of redshift. In both panels, data points are artificially shifted for clarity.

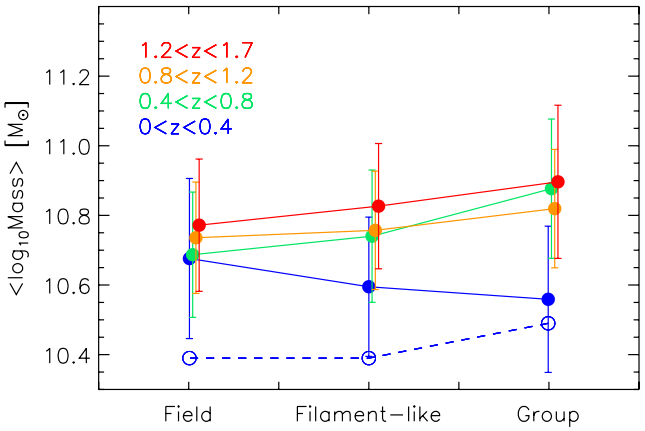

Figure 9. Comparison of mean stellar mass among group (within $2 \times R_{200}$), 'filament-like' and field galaxies. Data points are artificially shifted for clarity. Errors are derived using the mock catalogues of Kitzbichler & White (2007), as explained in the text. The dashed line represents the mean stellar mass for the different environments at $0 < z < 0.4$ for all galaxies with $M_* > 10^9\,M_\odot$. The normalization of the dashed line is artificially increased to higher value to make it close to the blue solid line only for comparison.

A mass cut at $M_* > 10^9\,M_\odot$ (dashed line and open symbols) allows us to highlight, once again, our spectroscopic bias on the lack of massive galaxies at low redshift. With the same mass cut, the $\langle SFR \rangle$ appears lower with respect to that derived with a higher mass cut at $M_* > 10^{10.3}\,M_\odot$ (dashed line and open symbols in Fig. 8), as expected by the MS evolution (e.g. Elbaz et al. 2007; Noeske et al. 2007a). Thus, we conclude that, even with this approach, the strong difference between groups and low-density regime observed at $z < 0.8$ is likely not ascribable to a strong mass segregation.

For completeness, we also analysed the evolution of the specific SFR (sSFR) density relation. This relation evolves in the same way as the SFR–density relation, since the mass–density relation is only slightly evolving.

3.3.1 Error analysis in the 'dynamical' approach

The errors on the mean SFR for group, 'filament-like' and field galaxies are estimated in a similar way as in Section 3.1.1. We randomly extract 100 catalogues (1000 regions with an area equal to the sum of the ECDFS and GOODS-N regions) in which we identify all haloes with masses between $10^{12.5}$ and $10^{14}\,M_\odot$ and all their members. This information is obtained by linking the mock catalogues of Kitzbichler & White (2007) to the parent halo properties provided by the 'friends-of-friends' algorithm (Davis et al. 1985) and the De Lucia et al. (2006) semi-analytic model tables of the Millennium data base. In the same regions, we define the 'filament-like' galaxies in the mock catalogues as the ones at the same density of the group galaxies but belonging to haloes with masses below $10^{12.5}\,M_\odot$. Finally, field galaxies are defined as sources with densities below the threshold in the real data set. We measure the mean SFR for group, 'filament-like' and field galaxies ($SFR_{\rm incomplete,\,group}$, $SFR_{\rm incomplete,\,filament}$ and $SFR_{\rm incomplete,\,field}$, respectively) by using the galaxy members of each respective environment as in the observational data set.

We measure in the same way the mean galaxy SFR ($SFR_{\rm real}$) for each population in the original (bias-free) Kitzbichler & White (2007) mock catalogues. We estimate, then, the difference $\Delta SFR = \log(SFR_{\rm real}) - \log(SFR_{{\rm incomplete},i})$ for each population, where $SFR_{{\rm incomplete},i}$ is the mean SFR of the given population in the ith region. The dispersion of the distribution of the residual ΔSFR provides the error on our mean SFR. This error takes into account the bias due to incompleteness, the cosmic variance (due to the fact that we are considering small areas of the sky) and the uncertainty in the mean due to a limited number of galaxies per redshift bin. The bias introduced by the spectroscopic selection leads to an overestimate of the mean SFR by the same amount, as expected, as in the case of the 'environmental approach'. The same overestimate is observed in each of the three populations. This is due to our assumption of a spatially uniform sampling rate as the one guaranteed by the spectroscopic coverage of the ECDFS and GOODS-N fields. The errors on the mean M_* are estimated with the same procedure used for retrieving the errors on the mean SFR for each population.

3.4 The SFR$-M_\star$ plane in different environments

In this section, we analyse the location of group, 'filament-like' and low-density (field) galaxies in the SFR–M_* plane. This is done

to identify the causes for the strong evolution of the SFR–density relation defined according to our 'dynamical' definition.

3.4.1 ΔMS and f_{QG} estimate

As already mentioned, Noeske et al. (2007a), Elbaz et al. (2007), Daddi et al. (2007) and several other authors find a well-defined sequence of star-forming galaxies in the SFR–M_* plane from $z \sim 0$ to 2. The relation shows a rather small scatter of 0.2–0.4 dex. The region below the MS is populated by quiescent galaxies (QGs) in a scattered cloud, while only a small fraction (2 per cent) of outliers is found to be located above (by a factor of 4) the MS in the starburst region (see Rodighiero et al. 2010).

Noeske et al. (2007b) suggest that the same set of physical processes governs the SF activity in galaxies on this smooth sequence. If 'mass quenching' (e.g. Peng et al. 2010) is the dominant mechanism for moving a galaxy off of the MS, the location of star-forming galaxies in high-density regions should not be different from that of the bulk of the star-forming galaxies in other environments. Conversely, if the environment plays a role in the evolution of the galaxy's SF activity, the position of the group galaxies along or across the MS should be different with respect to the bulk of the star-forming galaxies.

To shed light on this topic, we analyse the position of group, 'filament-like' and field galaxies with respect to the MS in the ECDFS and GOODS regions and in four redshift bins. In other words, we follow the behaviour of different environments defined in our dynamical approach (see Section 3.3) in the SFR–M_* plane.

Since the MS is well studied in the literature (e.g. Daddi et al. 2007; Elbaz et al. 2007; Noeske et al. 2007a; Peng et al. 2010), and the goal of this work is not to fit this relation again, we use the best-fitting relations available in the literature for the considered redshift bins. When no fit is available for a specific redshift bin, we interpolate the best-fitting relations of the two closest redshift bins.

Fig. 10 shows the SFR–M_* planes for the different redshift bins and above the mass threshold considered in this work. In each plot, the grey filled circles show the field galaxy population, while green and blue filled circles represent the 'filament-like' and group galaxy, respectively. We highlight with red empty circles all galaxies detected in the IR bands (>80 per cent) by PACS and MIPS. On the other hand, the SFRs derived via the SED fitting technique are useful for defining the cloud of quiescent or low-star-forming galaxies below the MS. The issue with this SFR estimator is that it can create artificial discreet trails when plotting SFR and M_*. However, we point out that this does not affect our study. In the lowest redshift bin only a few galaxies populate the SFR–M_* plane.

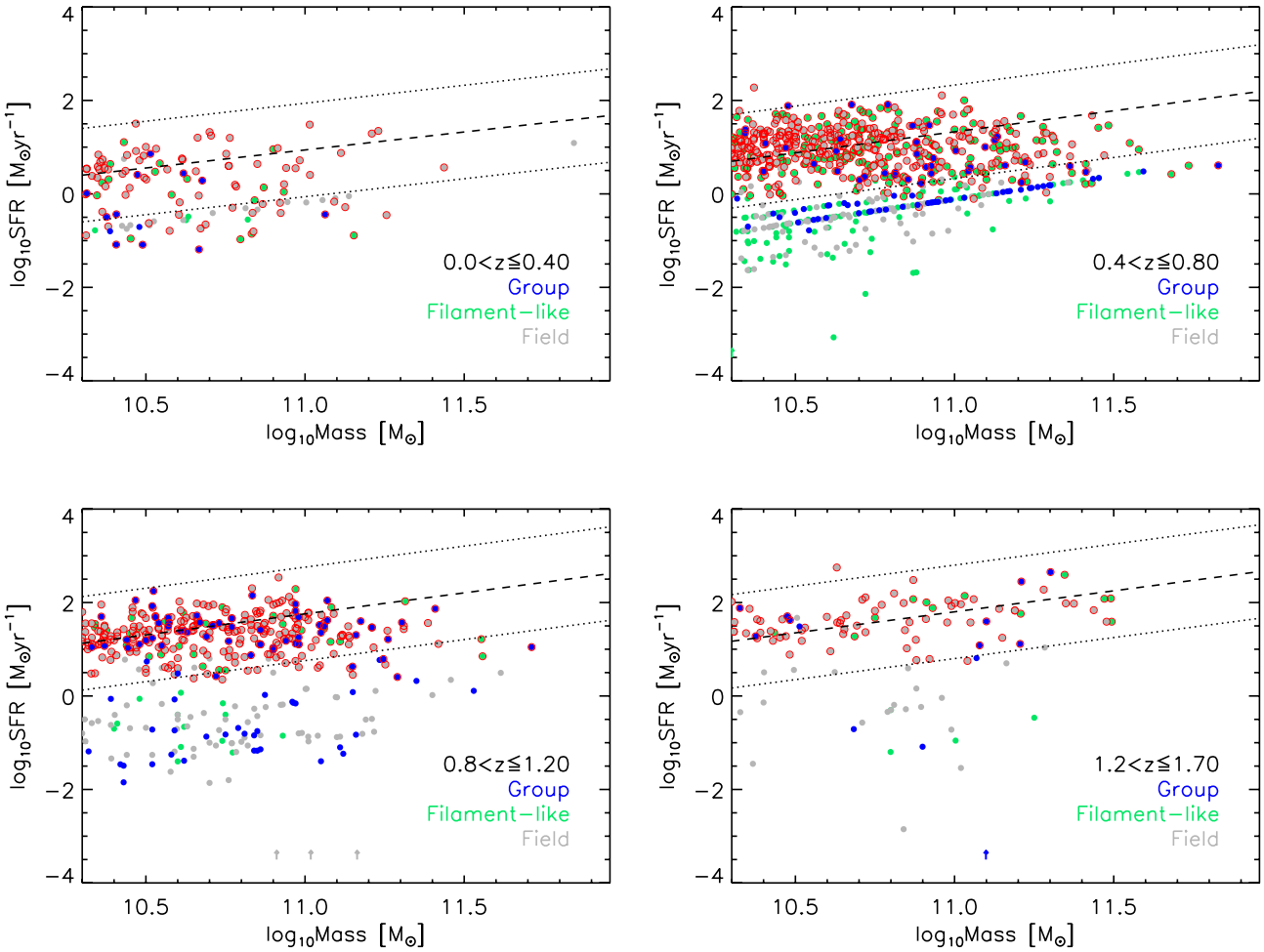

Figure 10. SFR−$M_\star$ diagrams for the different redshift bins considered in this work. We distinguish between group (blue filled circles), 'filament-like' (green filled circles) and field (grey filled circles) galaxies. The empty red circles represent all galaxies detected in the IR bands. The dashed lines show the MS relations from the literature as explained in the text. MS galaxies are selected within the dotted lines, while QGs are found below the dotted line, at lower SFR. The upward pointing arrows represent lower limits.

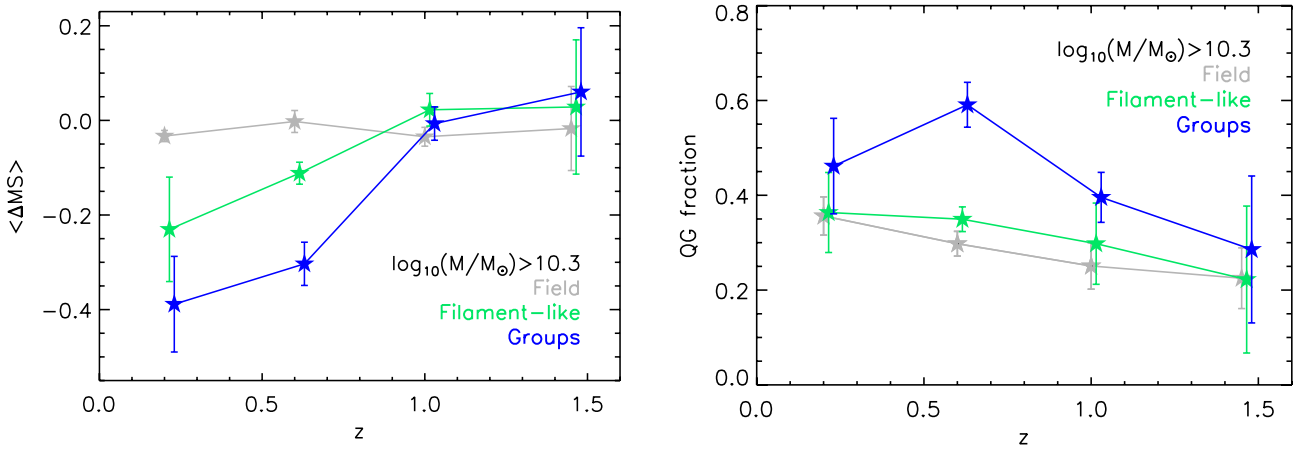

Figure 11. Left: evolution of the MS offset for group, 'filament-like' and field star-forming galaxies with $M_* > 10.3$. ΔMS represents the central value of the residuals with respect to the predicted MS for each redshift bin. Right: evolution of the QG fraction (f_{QG}) for group (blue stars), 'filament-like' (green stars) and field (grey stars) galaxies with $M_* > 10.3$. We define 'quiescent' all the galaxies with ΔMS < -1. In both panels, errors are derived using the mock catalogues of Kitzbichler & White (2007), as explained in the text and data points are artificially shifted for clarity.

This reflects the choice of giving a higher priority to spectroscopic targets like massive galaxies at high redshift (see Popesso et al. 2009; Z13).

In order to define the MS in the four redshift bins, we use the equations already used in the literature which best represent our data. In the $0 < z \leq 0.4$ redshift bin, we use an MS fit of Elbaz et al. (2007, their equation 5) based on SDSS star-forming galaxies at $z \sim 0$. At $0.4 < z \leq 0.8$ we do not find a fit in the literature, thus, we interpolate the MS relation of Peng et al. (2010) at $z \sim 0$ based on SDSS galaxies and that of Elbaz et al. (2007, their equation 4) at $z \sim 1$ based on *Spitzer* MIPS detected galaxies. The latter equation is used for the $0.8 < z \leq 1.2$ bin, with an offset[4] of log (SFR) $= -0.16$. As for the second redshift bin, the MS relation is not available in the literature for $1.2 < z \leq 1.7$. Thus, we interpolate between the Elbaz et al. (2007, their equation 4) MS relation at $z \sim 1$ and the MS relation at $z \sim 2$ of Daddi et al. (2007) based on UV data.

In all cases, we find a rather good agreement between our field galaxy distribution and the best-fitting relations, with the mean of the distribution peaked at ∼0 in the ΔMS residual at all redshifts (left-hand panel of Fig. 11). We define ΔMS $=$ log(SFR$_{\rm observed}$) $-$ log(SFR$_{\rm MS}$) as the residual of the SFR$-M_\star$ relation, where SFR$_{\rm observed}$ is the observed galaxy SFR and SFR$_{\rm MS}$ is the SFR predicted by the MS best fit. We estimate ΔMS for all the galaxies with mass above our mass cut ($M_* > 10^{10.3}\,{\rm M}_\odot$) and belonging to the three different environments in the usual redshift bins.

At this point, we identify and quantify the difference between the location across the MS of group galaxies in each bin with respect to the low-density and 'filament-like' galaxies. At all redshifts, the distribution of the ΔMS residuals shows a bimodal distribution: the Gaussian representing the MS location with a peak around 0, and a tail of quiescent/low-star-forming galaxies at low negative values of ΔMS. This distribution is reminiscent of the bimodal behaviour of the $u - r$ galaxy colour distribution observed by Strateva et al. (2001) in the SDSS galaxy sample. Following the example of Strateva et al. (2001), we identify the minimum value of the valley between the MS Gaussian and the peak of the broader quiescent/low-star-forming galaxies distribution. At all redshifts, the value ΔMS $= -1$ turns out to be the best separation between the two galaxy populations. Since the observed scatter of the MS at any redshift varies between 0.2 and 0.4 dex (Daddi et al. 2007; Elbaz et al. 2007), the limit at ΔMS $= -1$ should be consistent with a 3σ cut from the best-fitting MS relation. We use this value to separate MS galaxies from quiescent/low-star-forming galaxies in the three considered environments.

We measure the mean difference in SFR (ΔMS) from the MS location of the galaxy population in each environment, selecting only normally star-forming galaxies in the range $-1 \leq$ ΔMS ≤ 1. By definition, ΔMS should be consistent with 0 for the bulk of the MS galaxies. Thus, the mean of our Gaussian distribution centred around 0 confirms that our choice of the MS relation represents well the mean of the normally star-forming galaxies within our sample (but note that the slope might not be so well represented, see the end of Section 3.4.3). We stress once again that given the depth of the PACS and *Spitzer* MIPS observations of the ECDFS and GOODS fields, the MS is fully sampled (80 per cent) by IR-derived SFRs with very small (10 per cent) uncertainties. The SED fitting derived SFRs populate the region below the MS at ΔMS < -1, where we measure the QG fraction, f_{QG}. Thus, our estimate of the ΔMS should not be affected by the large error (0.5–0.6 dex) in the determination of the SFR via SED fitting (see Z13 for details).

3.4.2 *Error estimates of* ΔMS *and* f_{QG}

We estimate the error in ΔMS (f_{QG}) with the same approach used in Section 3.1.1. We use the usual 1000 regions with an area equal to the sum of the ECDFS and GOODS-N regions with a simulated spectroscopic incompleteness similar to our data set. We identify group, 'filament-like' and field galaxies in each region as explained in the error analysis of previous section.

Our aim is to apply the same technique used to analyse the real data set. Thus, we need the residual ΔMS with respect to the MS relation to measure the mean distance from the MS at $-1 <$ ΔMS < 1. However, the evolution of the MS predicted by the Kitzbichler & White (2007) catalogues is different from the one observed at the highest redshift considered in our work (see also Elbaz et al. 2007).

[4] This offset does not affect at all our results, but it is necessary to better represent the MS field galaxy population.

Indeed, simulated star-forming galaxies, in particular at high redshift, tend to be less star forming than in observations. Thus, the location of the MS using the mock catalogues at $z > 1$ tend to be below the observed MS in the same redshift bin. In order to cope with this problem, we change the normalization of the observed MS relation keeping the observed slope. Fitting the simulated MS provides similar results. In each area, we measure the mean distance from the MS at $-1 \leq \Delta\mathrm{MS} \leq 1$ as is done in the real data ($\langle \Delta MS_{\mathrm{incomplete}} \rangle$).

We follow the same procedure in the original and complete Kitzbichler & White (2007) mock catalogues by measuring $\Delta MS_{\mathrm{real}}$. We measure, then, the difference $\delta(\Delta\mathrm{MS}) = \Delta\mathrm{MS}_{\mathrm{real}} - \Delta\mathrm{MS}_{\mathrm{incomplete},i}$ for each population, where $\langle \Delta MS_{\mathrm{incomplete},i} \rangle$ is the residual of the considered population in the ith region. The dispersion of the distribution of the residual $\delta(\Delta\mathrm{MS})$ provides the error on the observed $\langle \Delta\mathrm{MS} \rangle$. As in the previous case, this error takes into account the bias due to incompleteness, the cosmic variance and the uncertainty in the measure of the mean due to a limited number of galaxies per redshift bin. We apply the same technique to estimate the f_{QG} error in each of the three populations at different redshift.

3.4.3 ΔMS and f_{QG} evolution

The left-hand panel of Fig. 11 shows the evolution of the $\langle \Delta\mathrm{MS} \rangle$ for the MS galaxies in low-density regions (grey stars and line), 'filament-like' environments (green stars and line) and groups (blue stars and line) up to $z \sim 1.6$. In the first two redshift bins, the $\langle \Delta\mathrm{MS} \rangle$ of the star-forming group galaxies is systematically below 0. At $z > 0.8$ the star-forming group galaxies are perfectly in sequence, consistently with the lower density environments. Moreover, the 'filament-like' MS galaxies appear to be placed between the low-density environment and the group galaxies.

This result shows, for the first time, that at least below $z \sim 0.8$ the SF activity in star-forming group galaxies is lower than in the bulk of the star-forming galaxies. Here, we show that a certain amount of pre-processing (galaxies being pre-processed in groups before entering clusters; Zabludoff & Mulchaey 1998) happens even before star-forming galaxies enter the group environment. In fact, some quenching is already in place when galaxies fall along filaments or lower mass groups that could eventually merge to form more massive structures. Thus, the speed of the evolution of the SF activity in star-forming galaxies depends, at least since $z \sim 1$, on the galaxy environment.

For completeness of the analysis, we also investigate the evolution of the galaxy-type mix for each environment. The galaxy-type mix is expressed through the fraction of QGs, f_{QG}. As already mentioned, we define as QGs all those systems with $\Delta\mathrm{MS} < -1$, i.e. all the sources in the cloud below the MS. The right-hand panel of Fig. 11 shows the evolution of f_{QG} in the three environments. Low-density (grey stars and line) and 'filament-like' galaxies (green stars and line) exhibit the same galaxy-type mix at any redshift and no evolution is observed in these environments at least in the mass range considered in our analysis. The galaxy-type mix in groups exhibits a higher f_{QG} with respect to the other two environments, at any redshift. We note that the first redshift bin is affected by the spectroscopic selection function of our sample. The evolution of f_{QG} is stronger in groups that in the other environments. In particular, we note that at $z \sim 0.8$ the fraction of QGs is twice the mean fraction observed at high redshift.

The two panels of Fig. 11 show two different aspects of the role of environment in the evolution of galaxy SF activity. Some degree of partial quenching is observed as suggested by the 'environmental gradient' as a function of distance from the MS. On the other hand, the right-hand panel shows that the density is not responsible for the different galaxy-type mix. Indeed the group- and 'filament-like' regimes cover, by definition, the same range of local galaxy density. The main difference is that, in the group regime, galaxies likely belong to a massive ($M_{200} \sim 2 \times 10^{13}\,\mathrm{M}_{\odot}$, see Z13 for the sample mass distribution) bound dark matter halo, while in the 'filament-like' regime galaxies likely belong to unbound structures, such as filaments or lower mass haloes. Thus, the different evolution of the galaxy-type mix of the two environments, similar in projected density but not in dynamical properties, indicates that a high f_{QG} requires a massive parent dark matter halo rather than simply an overdensity of galaxies.

In order to verify that our result is robust, we perform some sanity checks. This choice is driven by the distribution of galaxies in the SFR$-M_{\star}$ plane. In fact, massive galaxies lie mainly below the MS (as defined, see Fig. 10), with the locus of galaxies apparently steepening towards lower SFR (see e.g. Noeske et al. 2007b; Whitaker et al. 2012). Thus, a non-zero ΔMS could result from an environmental dependent distribution of mass coupled with an MS relation which does not represent the data at all masses. The Kolmogorov–Smirnov test reveals that the mass distributions of star-forming galaxies in different environments are consistent with one another in all redshift bins, except the second one. This could be a problem since a more significant population of the most massive galaxies is expected in groups compared to the field. To check how our findings are affected by this issue, we investigate the evolution of ΔMS and f_{QG} in two different stellar mass bins: $10^{10.3} < M_*/\mathrm{M}_{\odot} < 10^{10.9}$ and $10^{10.9} < M_*/\mathrm{M}_{\odot} < 10^{12}$ (Fig. 12). Reassuringly, we find results consistent with Fig. 11. We note that the lowest redshift bin is populated by only a few galaxies and so we focus on higher redshifts.

In general, in the low-mass bin we observe a similar trend in ΔMS and f_{QG} as in the total sample, while in the high-mass bin ΔMS is systematically below 0 (bottom-left panel of Fig. 12). This illustrates that massive star-forming galaxies are not well represented by a linear MS relation (cf. Whitaker et al. 2012). However, since the evolution of ΔMS for the other environments is similar to the total sample, we conclude that the relative offset observed in Fig. 11 for 'filament-like' and group galaxies is real. Also the evolution of f_{QG} remains similar to the total sample in both stellar mass bins. Even though it is less populated than the low-mass bin, the high-mass bin better highlights the different quenching in groups, 'filament-like' environment and field.

4 DISCUSSION

4.1 The SFR–density relation

We have investigated the SFR–density relation using two different approaches. One, more traditional, studies the relation between SFR and density for all galaxies, while the other (the 'dynamical' approach) isolates the contribution of group galaxies with respect to other environments in the SFR–density relation.

Our results show that the SFR–density relation has progressively lower significance towards high redshift, but it does not reverse at $z \sim 1$. In addition, a careful analysis of the biases due to the spectroscopic selection leads to the conclusion that we can also not exclude an anticorrelation at $z \gtrsim 1$. The observed SFR–density anticorrelation at $z < 0.8$ is not simply ascribable to mass segregation (most massive galaxies are generally passive galaxies, low-mass galaxies

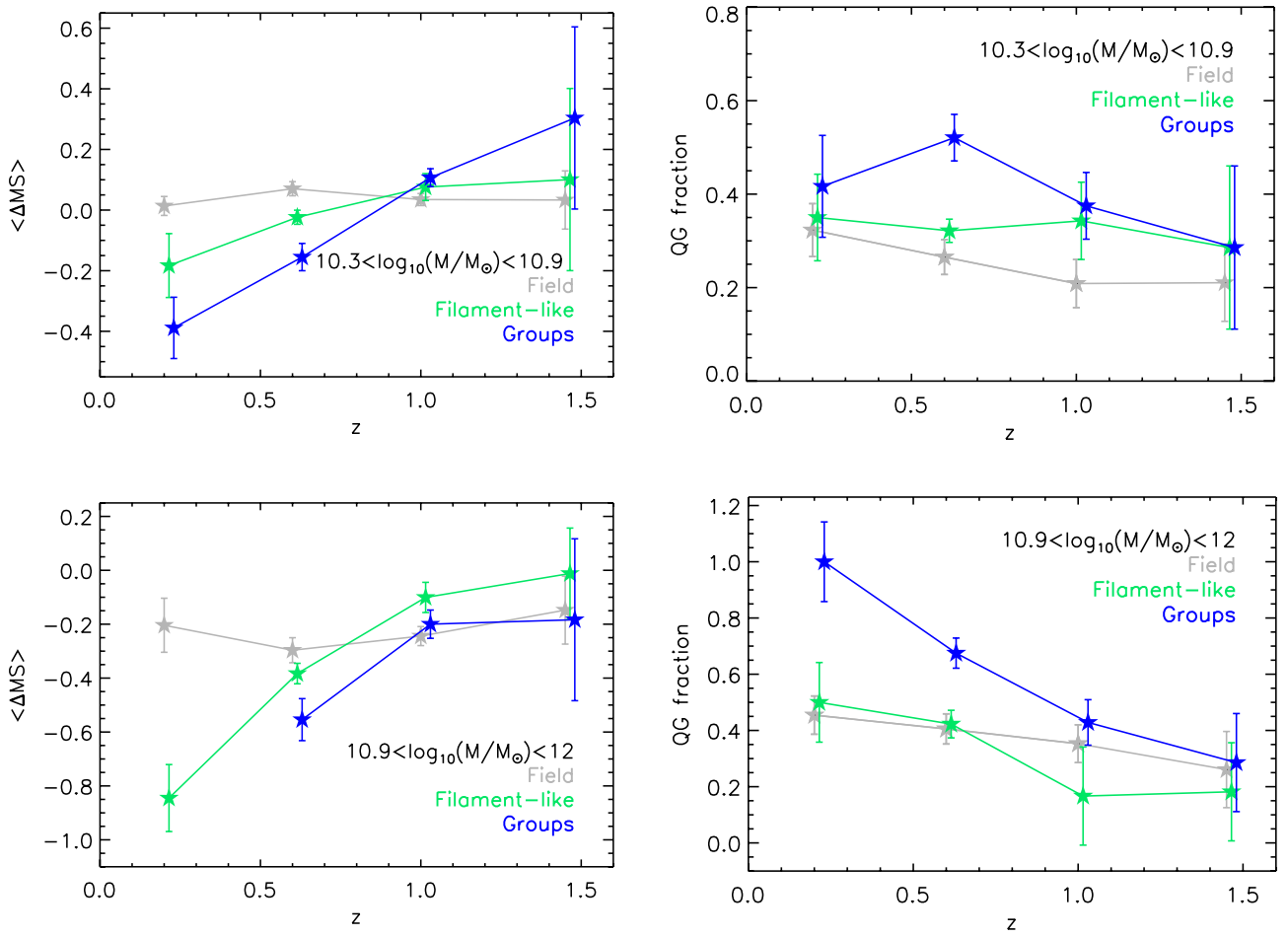

Figure 12. Left-hand column: evolution of the MS offset for group, 'filament-like' and field star-forming galaxies with $10.3 < \log(M_\star/\mathrm{M}_\odot) < 10.9$ and $10.9 < \log(M_\star/\mathrm{M}_\odot) < 12$ (top and bottom, respectively). Right-hand column: evolution of f_{QG} for group (blue stars), 'filament-like' (green stars) and field (grey stars) galaxies for the same range of stellar mass as in the left-hand column. In all panels, errors are derived using the mock catalogues of Kitzbichler & White (2007), as explained in the text and data points are artificially shifted for clarity.

are, on average, star forming). Indeed, we observe only a mild mass segregation in any redshift bin.

Our results seem to be at odds with Kauffmann et al. (2004) who find strong mass segregation at least in the local Universe. At higher redshift the effect has never been thoroughly analysed, except for the results of Scodeggio et al. (2009) and Bolzonella et al. (2010) who showed that already at $z \sim 1$ mass and galaxy density are coupled with the most massive galaxies segregated in the most dense environment. We must note that our stellar mass cut ($M_* > 10^{10.3}\,\mathrm{M}_\odot$) is rather high. Indeed, a lower mass cut ($M_* > 10^9\,\mathrm{M}_\odot$) in the lowest redshift bin leads to a stronger mass segregation, although of small amplitude. This would be in agreement with the recent finding of Rasmussen et al. (2012), who observe mass segregation within 10 R_{200} for groups, by only considering low-mass galaxies.

Given the flattening of the SFR–density relation observed after excluding group galaxies from the sample, we conclude that group members are mostly responsible for the observed anticorrelation at $z < 0.8$. Thus, galaxies living in relatively massive dark matter haloes must have a suppressed mean SFR with respect to the field, at least up to $z \sim 0.8$. This is confirmed by the SFR–density relation analysed with our 'dynamical' approach.

One of the most striking findings in our analysis is the lack of reversal of the SFR–density relation at $z \sim 1$. This result is at odds with recent findings. In particular, Elbaz et al. (2007) and Cooper et al. (2008) observe the reversal of the SFR–density relation at $z \sim 1$ in the GOODS and the DEEP2 fields, respectively, using a spectroscopically defined density parameter. We have extensively compared our analysis with that of Elbaz et al. (2007) and Popesso et al. (2011), since our data set includes the sky regions analysed in their data set (Fig. 7). In particular, we have considered the possibility that the fraction of AGN could affect the SFR estimate. In fact, since the fraction of AGN is found to be higher in groups as the redshift increases (Georgakakis et al. 2007; Georgakakis 2008; Tanaka et al. 2012) and the SFR of AGN host galaxies could be enhanced with respect to non-active galaxies of similar stellar mass (Santini et al. 2012; Rosario et al. 2013), we use PACS data to measure, without biases, their SFR (Popesso et al. 2011). This cannot be done using MIPS data or the [O II] doublet. Removing the AGN from our sample does not affect the significance of the SFR–density relation. This could be due to cosmic variance, since the fraction of AGN present in the GOODS-S field is higher (17 per cent in the highly star-forming galaxies; Popesso et al. 2011) with respect to ECDFS and GOODS-N (3–5 per cent).

Finally, we consider the possibility that the density definition itself could be responsible for the differences we observe. In fact, as explained in Section 2.2, our density estimate is based on a stellar mass cut. Popesso et al. (2012) show that the density definition adopted by Elbaz et al. (2007), based on a galaxy apparent

magnitude cut ($z_{AB} < 23.5$ mag), could lead to a strong redshift bias. Thus, we conclude that the previously observed reversal of the SFR–density relations is most likely due to the combination of different effects: the galaxy sample selection, high fraction of AGN and a possibly biased definition of the density parameter, which can hide a redshift dependence.

Our results are, instead, in agreement with Feruglio et al. (2010), who find no dependence of the SFR and LIRG fraction on environment, arguing that the reversal, if any, must occur at $z > 1$. According to Feruglio et al. (2010), the reversal found by Elbaz et al. (2007) and Cooper et al. (2008) might be due to the contribution of galaxies at lower stellar mass and SFR comprised in Elbaz et al. (2007) and Cooper et al. (2008) galaxy sample. However, since we consider a wide range of SFR and M_*, we disagree with this conclusion. The advantage of the Feruglio et al. (2010) study is the use of COSMOS data, which, due to its wide field, is less affected by cosmic variance [although Cooper et al. (2008) is the least impacted, covering a larger volume spread over four distinct fields]. On the other hand, it must be noted that the authors use sources with both spectroscopic and photometric redshifts to define the density field. This could dilute any overdensity present in the field. Our approach is, therefore, more rigorous in this sense.

In our analysis, we estimated the SFR using both IR data and multiwavelength SED fitting. The latter is used for all galaxies undetected in the IR bands, i.e. below the MS. This SFR estimator gives a larger uncertainty with respect to the IR data, as shown in Z13. However, in the case of an underestimate of the $\mathrm{SFR_{SED}}$, i.e. for all galaxies that would be on the MS, we should have an IR detection, thus a more robust SFR estimate. On the other hand, in case $\mathrm{SFR_{SED}}$ overestimates the real value, the signal could be washed out (Cooper et al. 2010). For example, any anticorrelation at $z > 0.8$ could be hidden by the errors. In fact, as shown also by Wuyts et al. (2011), the uncertainties on the SFR (SED) increase as a function of redshift.

We discuss our possible biases by using the mock catalogues of Kitzbichler & White (2007). In all cases, we measure an $\langle \mathrm{SFR} \rangle$ higher than the one predicted by the simulations. This comparison also assures that we are not suffering from any bias in the slope of the SFR–density relation and, thus, that our results are robust. Moreover, we note that in some cases the cosmic variance (or the big uncertainty in the $\mathrm{SFR_{SED}}$) could wash out the signal in the SFR–density anticorrelation in the highest redshift bins.

The use of the standard approach for the study of the SFR–density relation, can be ineffective if the local galaxy density is not directly connected to the SF activity, due either to mass segregation or to SF quenching processes linked to galaxy–galaxy interactions. For this reason, we analyse the SFR–density relation with a novel 'dynamical' approach. This technique allows us to separate the contribution to the highest galaxy density bins of groups and 'filament-like' galaxies. This is not possible in a more classical 'environmental approach' (although see Wilman et al. 2010).

Our results show that the bulk of the SF is quenched in groups. This is what drives the trend of the SFR–density relation. The 'filament-like' environment has a slower evolution in SF compared to the groups, thus the density (galaxy–galaxy interaction) itself cannot be responsible for the bulk of the quenching. We note that we use a fairly large velocity window to compute densities, much larger than the typical velocity differences at which galaxy–galaxy interactions are effective. This means that there can be a certain dynamic range in the efficiency of our density estimates. In the X-ray groups, galaxies have typically smaller velocity differences than chance projections, but larger differences than close pairs. Both the latter types contribute to 'filament-like' environments.

This result is not necessarily inconsistent with Z13. In Z13, we show that the SF activity of galaxies is not affected by the local environment of groups, but here we find that it does depend on the global environment. In other words, the level of SF activity is generally low in groups (with respect to the other environments) even if it is independent from the group-centric distance (and from the density, as discussed in Z13). Rather than being inconsistent with Z13, this strengthens our results. In fact, we show, once again, that the density is not responsible for the bulk of the quenching (although we cannot exclude that some quenching is happening for galaxy–galaxy interactions), but that processes related to a massive dark matter halo are more effective.

The high SFR in the 'filament-like' galaxies at low redshift, more consistent with the field than with the group $\langle \mathrm{SFR} \rangle$, is in agreement with the recent finding of Fadda et al. (2008) and Biviano et al. (2011). They show that the filament around the supercluster A1763 hosts the highest fraction of IR-emitting galaxies. Similarly, the 'filament-like' region contains the highest total SFR per unit galaxy. Our findings are also consistent with those of Porter & Raychaudhury (2007), who have used optical data to discover an enhanced star-forming activity among galaxies associated with filaments in the nearby Pisces–Cetus supercluster.

4.2 The SFR$-M_\star$ plane in different environments

In order to investigate the cause of the strong evolution of SF activity in our sample, we have studied the position of group, 'filament-like' and field star-forming galaxies with respect to the MS galaxy population (Daddi et al. 2007; Elbaz et al. 2007; Noeske et al. 2007a; Peng et al. 2010).

Many works focus mainly on the study of the MS in field galaxies. For example, according to Noeske et al. (2007b), this sequence suggests that the same small set of physical processes governs the SF activity in galaxies. Thus, if galaxy evolution is driven mainly by their *nature*, there should be no difference among MS star-forming galaxies, regardless of their environment. On the other hand, if a galaxy depends on the environment in which it lies, a group member should have a different level of SF with respect to the bulk of star-forming galaxies on the MS.

This last point reflects our main result from the analysis of the SFR$-M_\star$ relation. In particular, we have studied, for the first time, the location of galaxies in different environments on the SFR$-M_\star$ plane. The evolution of $\langle \Delta\mathrm{MS} \rangle$ shows that, at least below $z \sim 0.8$, the SF activity in group galaxies is quenched with respect to the bulk of star-forming galaxies. At earlier epochs, group, 'filament-like' and field galaxies have comparable SF. Interestingly, the density seems to play a role in the distance from the MS, since the filaments represent a somewhat intermediate environment in the evolution of $\langle \Delta\mathrm{MS} \rangle$. Therefore, we show, with high significance, that the speed of the evolution of SF activity in star-forming galaxies depends, at least since $z \sim 1$, on the galaxy environment, defined according to our 'dynamical' approach. In addition, we find that the fraction of QGs, f_{QG}, evolves faster in groups with respect to both filaments and field. The latter two environments show a similar evolution of f_{QG}. This confirms that quenching processes related to a rather massive dark matter halo ($\gtrsim 2 \times 10^{13}\,\mathrm{M_\odot}$) are more efficient than those associated with a generally dense region. Thus, strangulation (Larson, Tinsley & Caldwell 1980), ram pressure stripping (Gunn & Gott 1972) and harassment (Moore et al. 1996) are likely to be much more effective than the simple galaxy–galaxy interaction.

Our result is in contrast with the analysis of Peng et al. (2012). These authors argue that central star-forming galaxies are equivalent to field galaxies. They claim that there is no difference in the MS relation of central and satellite galaxies. However, it is not clear how they discern between star-forming and passive galaxies. In fact, over their whole study, Peng et al. (2012) use the red/blue galaxy dichotomy to distinguish between passive/star-forming galaxies, respectively. As shown by Woo et al. (2013), about 30 per cent of the SDSS red sequence galaxies, identified in the colour-magnitude diagram, lie on the MS, which is also populated by green valley galaxies (Rosario et al. 2013). Whitaker et al. (2012) confirm this point, finding two different MS for blue and star-forming galaxies. This implies that selecting blue galaxies misses many red, dusty, star-forming sources. Moreover, Peng et al. (2012) use the catalogue of Yang et al. (2007, based on a friends-of-friends algorithm) to explore the properties of group galaxies. As we already mentioned, optical selection of group is much more prone to projection effects than X-ray selection. In fact, the optically selected group catalogues do not contain virialized, relatively high-mass, X-ray-emitting groups and include many more low-mass and unvirialized groups, as well as some pure projections. Finally, (part of) optically selected groups could be classified as 'filament-like' galaxies, implying an $f_{\rm QG}$ evolution similar to that of field galaxies.

Recently, Rasmussen et al. (2012), computing the SFR from UV emission for nearby group galaxies, found an MS broadly consistent but flatter than the MS of field galaxies at the same redshift. They argue that a flattening could be expected if the SFR of low-mass galaxies is suppressed in groups. At a median mass of $\log(M_\star/{\rm M}_\odot) = 9.63$, their MS predicts a mean sSFR which is ∼40 per cent lower than that expected for the field. This could be consistent with our results, although we do not cover the same mass range.

Our findings support the pre-processing scenario (galaxies age in groups before entering clusters; Zabludoff & Mulchaey 1998). This is consistent with the result of Wilman et al. (2008), who find a strong suppression of SF activity in a sample of $z \sim 0.4$ groups. They estimate a stronger quenching for galaxies with $M_* \gtrsim 10^{11}\,{\rm M}_\odot$, where the fraction of star-forming galaxies falls down to ∼12 per cent. Our results are also in agreement with an analogous analysis done by Bai et al. (2010) on the sample of 2dF groups. The authors show that the group star-forming galaxies are located below the field MS, but above the location of the bulk of cluster star-forming galaxies. This suggests that, although some pre-processing is present in groups, a stronger quenching must happen in more dense and massive systems, like clusters. In this work, we also show that a certain amount of pre-processing happens when galaxies are falling along the filaments, before they enter the group environment. However, halo-related processes seem to be more effective in quenching the SF.

The pre-processing scenario is also supported by models. De Lucia et al. (2012), using semi-analytic models, show that the fraction of galaxies that can be pre-processed in a group-size halo of mass $\sim 10^{13}\,{\rm M}_\odot$ is significant (∼27 per cent which raise to ∼44 per cent for galaxies with $M \sim 10^{11}\,{\rm M}_\odot$). Furthermore, comparing observations with their theoretical predictions, they argue that satellite galaxies become passive after they have spent 5–7 Gyr in haloes more massive than $M_{\rm halo} \sim 10^{13}\,{\rm M}_\odot$. Similarly, McGee et al. (2009), using the stellar masses and merger trees produced by the semi-analytic galaxy catalogues, suggest that all clusters in their sample exhibit a significant fraction of their galaxies accreted through galaxy groups. For instance, they propose that this fraction is 40 per cent for $10^{14.5}\,{\rm M}_\odot$ clusters at $z = 0$ and only ∼25 per cent at higher redshifts ($z \sim 1.5$). Our results show qualitative agreement with this prediction. Conversely, Berrier et al. (2009), using cosmological ΛCDM *N*-body simulations, suggest that on average, ∼70 per cent of cluster galaxies fall into the cluster potential directly from the field. On the other hand, less than ∼12 per cent of cluster galaxies are accreted as members of groups with five or more galaxies.

The pre-processing scenario is also reflected in our analysis on the QGs fraction in groups, 'filament-like' environments and field. Our findings suggest that these environments have a different galaxy-type mix up to $z \sim 1$, with groups being the most efficient at quenching the SF. At higher redshift, the galaxy population of groups, filaments and field is similar.

Our results find support in several works in the literature. For example, Kovač et al. (2010) show that galaxy SF and colour transformation rates are higher in the group regions than in lower density areas at $z \sim 1$. In addition, Presotto et al. (2012) suggest that galaxy colours are particularly affected by the group environment (with respect to the field) on short time-scales in a redshift range $0.2 < z < 0.8$. Finally, Iovino et al. (2010) and Gerke et al. (2007) show that the group galaxy population becomes bluer as the redshift increases, but it maintains a systematic difference with respect to the global galaxy population, and an even larger difference with respect to the isolated galaxy population.

5 SUMMARY AND CONCLUSIONS

In this work, we have investigated the SFR–density relation in different environments up to $z \sim 1.6$. We have used multiwavelength data from the ECDFS and GOODS fields to study the evolution of SF activity in four redshift bins. Moreover, the use of deep MIPS 24 μm and *Herschel* PACS data has assured an accurate estimate of the SFR for all detected IR sources (in particular MS galaxies). This rich data set has enabled the use of two different approaches to investigate the evolution of the SFR–density relation: an 'environmental' approach, which is the traditional method used in the literature, and a novel 'dynamical' approach, which splits the sample into group, 'filament-like' and field galaxies.

By studying the SFR–density relation in the standard way, we have found an anticorrelation up to $z \sim 0.8$ but no correlation at higher redshift. Although the significance found by the Spearman test decreases as the redshift increases, we did not observe any reversal of the SFR–density relation. After checking for the presence of biases using the mock catalogues of Kitzbichler & White (2007), we have verified that we have constantly overestimated the values of SFR at all redshifts, due to the spectroscopic incompleteness of our catalogues, but that the slope of our SFR–density relation is not affected by any bias. We have also found that the role of AGN is rather marginal in shaping the relation and that the anticorrelation at $z < 0.8$ is dominated by spectroscopic group members. Since our galaxy sample shows only a mild mass segregation at any redshift bin, we conclude that the SFR–density relation is not driven by a strong mass segregation.

By using the 'dynamical' definition of environment, we have asserted that the bulk of quenching happens in groups. Indeed, group spectroscopic members show a much lower mean SFR than galaxies at similar density but not belonging to bound structures, at least up to $z \sim 1$. On the other hand, galaxies in unbound structures exhibit a similar evolution of SFR as field isolated galaxies. Group galaxies only reach the same level of SF activity as field galaxies at

$z > 1$. However, even with this alternative approach, we have not detected any significant SFR–density reversal. Thus, we conclude that group galaxies experience a much faster evolution with respect to galaxies in other environments. In addition, the strong difference in the evolution of the group galaxies with respect to non-group galaxies at similar density (i.e. 'filament-like') reveals that processes related to the presence of a massive dark matter halo (ram pressure stripping, strangulation and harassment) must be dominant in the suppression of the SF activity in group galaxies below $z \sim 1$. On the other hand, purely density-related processes (close encounters and tidal stripping) play a secondary role in the quenching.

In order to understand the cause of the faster evolution in group galaxies, we have also studied the location of group, 'filament-like' and field galaxies in the SFR$-M_\star$ plane. This has been done to identify if the lower $\langle$SFR$\rangle$ in groups at $z < 1$ with respect to field galaxies is due to a general quenching of the SF in all galaxies or to a faster evolution of the galaxy-type mix. We have found that the MS of group galaxies is offset with respect to that of field galaxies up to $z \sim 0.8$, i.e. it is shifted towards lower SFRs. At higher redshift the star-forming group galaxies are in sequence. 'Filament-like' galaxies occupy a half-way position between groups and field. This suggests that both the density- and halo-related processes are playing a role in quenching the SF activity of actively star-forming galaxies, but that density seems to play a secondary role. Interestingly, the QGs fraction evolves faster in groups than in the other two environments up to $z \sim 0.8$, beyond which the fractions are comparable. We conclude that the strong evolution observed in the SFR–density relation, analysed in the dynamical approach, is likely to be the driver of the different galaxy-type mix in groups across cosmic epochs.

ACKNOWLEDGEMENTS

We thank the anonymous referee for her/his constructive comments.

FZ acknowledges the support from and participation in the International Max-Planck Research School on Astrophysics at the Ludwig-Maximilians University.

We would like to thank Rob Yates for reading the paper and providing useful comments.

MT gratefully acknowledges support by KAKENHI no. 23740144.

FEB acknowledges support from Basal-CATA (PFB-06/2007), CONICYT-Chile (under grants FONDECYT 1101024, ALMA-CONICYT 31100004 and Anillo ACT1101), and *Chandra* X-ray Center grant SAO SP1-12007B.

PACS has been developed by a consortium of institutes led by MPE (Germany) and including UVIE (Austria); KUL, CSL, IMEC (Belgium); CEA, OAMP (France); MPIA (Germany); IFSI, OAP/AOT, OAA/CAISMI, LENS, SISSA (Italy); and IAC (Spain). This development has been supported by the funding agencies BMVIT (Austria), ESA-PRODEX (Belgium), CEA/CNES (France), DLR (Germany), ASI (Italy) and CICYT/MCYT (Spain).

This research has made use of NASA's Astrophysics Data System, of NED, which is operated by JPL/Caltech, under contract with NASA, and of SDSS, which has been funded by the Sloan Foundation, NSF, the US Department of Energy, NASA, the Japanese Monbukagakusho, the Max Planck Society, and the Higher Education Funding Council of England. The SDSS is managed by the participating institutions (www.sdss.org/collaboration/credits.html).

This work has been partially supported by a SAO grant SP1-12006B grant to UMBC.

REFERENCES

Arnouts S. et al., 2001, A&A, 379, 740
Bai L., Rasmussen J., Mulchaey J. S., Dariush A., Raychaudhury S., Ponman T. J., 2010, ApJ, 713, 637
Balestra I. et al., 2010, A&A, 512, A12
Barger A. J., Cowie L. L., Wang W.-H., 2008, ApJ, 689, 687
Berrier J. C., Stewart K. R., Bullock J. S., Purcell C. W., Barton E. J., Wechsler R. H., 2009, ApJ, 690, 1292
Biviano A., Fadda D., Durret F., Edwards L. O. V., Marleau F., 2011, A&A, 532, A77
Bolzonella M. et al., 2010, A&A, 524, A76
Bruzual G., Charlot S., 2003, MNRAS, 344, 1000
Cardamone C. N. et al., 2010, ApJS, 189, 270
Chabrier G., 2003, PASP, 115, 763
Cooper M. C., Newman J. A., Madgwick D. S., Gerke B. F., Yan R., Davis M., 2005, ApJ, 634, 833
Cooper M. C. et al., 2008, MNRAS, 383, 1058
Cooper M. C. et al., 2010, MNRAS, 409, 337
Cooper M. C. et al., 2012, MNRAS, 425, 2116
Daddi E. et al., 2007, ApJ, 670, 156
Davis M., Efstathiou G., Frenk C. S., White S. D. M., 1985, ApJ, 292, 371
De Lucia G., Springel V., White S. D. M., Croton D., Kauffmann G., 2006, MNRAS, 366, 499
De Lucia G., Weinmann S., Poggianti B. M., Aragón-Salamanca A., Zaritsky D., 2012, MNRAS, 423, 1277
Dressler A., 1980, ApJ, 236, 351
Elbaz D. et al., 2007, A&A, 468, 33
Elbaz D. et al., 2011, A&A, 533, A119
Fadda D., Biviano A., Marleau F. R., Storrie-Lombardi L. J., Durret F., 2008, ApJ, 672, L9
Fazio G. G. et al., 2004, ApJS, 154, 10
Feruglio C. et al., 2010, ApJ, 721, 607
Finoguenov A. et al., 2007, ApJS, 172, 182
Finoguenov A. et al., 2009, ApJ, 704, 564
Georgakakis A., 2008, Astron. Nachr., 329, 174
Georgakakis A. et al., 2007, ApJ, 660, L15
George M. R. et al., 2011, ApJ, 742, 125
George M. R. et al., 2012, ApJ, 757, 2
Gerke B. F. et al., 2007, MNRAS, 376, 1425
Giavalisco M. et al., 2004, ApJ, 600, L93
Gómez P. L. et al., 2003, ApJ, 584, 210
Grazian A. et al., 2006, A&A, 449, 951, 1
Gunn J. E., Gott J. R., III, 1972, ApJ, 176, 1
Ideue Y. et al., 2009, ApJ, 700, 971
Ideue Y. et al., 2012, ApJ, 747, 42
Ilbert O. et al., 2006, A&A, 457, 841
Ilbert O. et al., 2010, ApJ, 709, 644
Iovino A. et al., 2010, A&A, 509, A40
Kauffmann G., White S. D. M., Heckman T. M., Ménard B., Brinchmann J., Charlot S., Tremonti C., Brinkmann J., 2004, MNRAS, 353, 713
Kewley L. J., Geller M. J., Jansen R. A., 2004, AJ, 127, 2002
Kitzbichler M. G., White S. D. M., 2007, MNRAS, 376, 2
Kovač K. et al., 2010, ApJ, 708, 505
Kurk J. et al., 2009, A&A, 504, 331
Larson R. B., Tinsley B. M., Caldwell C. N., 1980, ApJ, 237, 692
Lewis I. et al., 2002, MNRAS, 334, 673
Lutz D. et al., 2010, ApJ, 712, 1287
McGee S. L., Balogh M. L., Bower R. G., Font A. S., McCarthy I. G., 2009, MNRAS, 400, 937
Magnelli B., Elbaz D., Chary R. R., Dickinson M., Le Borgne D., Frayer D. T., Willmer C. N. A., 2011, A&A, 528, A35
Magnelli B. et al., 2013, A&A, 553, A132
Moore B., Katz N., Lake G., Dressler A., Oemler A., 1996, Nat, 379, 613
Muldrew S. I. et al., 2012, MNRAS, 419, 2670
Muzzin A. et al., 2012, ApJ, 746, 188
Netzer H. et al., 2007, ApJ, 666, 806
Noeske K. G. et al., 2007a, ApJ, 660, L43

Noeske K. G. et al., 2007b, ApJ, 660, L47
Peng Y. et al., 2010, ApJ, 721, 193
Peng Y.-j., Lilly S. J., Renzini A., Carollo M., 2012, ApJ, 757, 4
Poglitsch A. et al., 2010, A&A, 518, L2
Popesso P. et al., 2009, A&A, 494, 443
Popesso P. et al., 2011, A&A, 532, A145
Popesso P. et al., 2012, A&A, 537, A58
Porter S. C., Raychaudhury S., 2007, MNRAS, 375, 1409
Presotto V. et al., 2012, A&A, 539, A55
Rasmussen J., Mulchaey J. S., Bai L., Ponman T. J., Raychaudhury S., Dariush A., 2012, ApJ, 757, 122
Rettura A. et al., 2010, ApJ, 709, 512
Rodighiero G. et al., 2010, A&A, 518, L25
Rosario D. J. et al., 2013, ApJ, 771, 63
Santini P. et al., 2012, A&A, 540, A109
Scodeggio M. et al., 2009, A&A, 501, 21
Scoville N. et al., 2007, ApJS, 172, 1
Shao L. et al., 2010, A&A, 518, L26
Silverman J. D. et al., 2010, ApJS, 191, 124
Springel V. et al., 2005, Nat, 435, 629
Strateva I. et al., 2001, AJ, 122, 1861
Tanaka M., Lidman C., Bower R. G., Demarco R., Finoguenov A., Kodama T., Nakata F., Rosati P., 2009, A&A, 507, 671
Tanaka M. et al., 2012, PASJ, 64, 22
Tran K.-V. H. et al., 2010, ApJ, 719, L126
Whitaker K. E., van Dokkum P. G., Brammer G., Franx M., 2012, ApJ, 754, L29
Wilman D. J. et al., 2008, ApJ, 680, 1009
Wilman D. J., Zibetti S., Budavári T., 2010, MNRAS, 406, 1701
Woo J. et al., 2013, MNRAS, 428, 3306
Wuyts S. et al., 2011, ApJ, 742, 96
Xue Y. Q. et al., 2011, ApJS, 195, 10
Yang X., Mo H. J., van den Bosch F. C., Pasquali A., Li C., Barden M., 2007, ApJ, 671, 153
York D. G. et al., 2000, AJ, 120, 1579
Zabludoff A. I., Mulchaey J. S., 1998, ApJ, 496, 39
Ziparo F. et al., 2013, MNRAS, 434, 3089 (Z13)

This paper has been typeset from a TEX/LATEX file prepared by the author.